



11 **ABSTRACT**

12 Ciliary assembly, trafficking, and regulation are dependent on microtubules, but the  
13 mechanisms of ciliary assembly also require the actin cytoskeleton. Here, we dissect subcellular  
14 roles of actin in ciliogenesis by focusing on actin networks nucleated by the Arp2/3 complex in  
15 the powerful ciliary model, *Chlamydomonas*. We find the Arp2/3 complex is required for the  
16 initial stages of ciliary assembly when protein and membrane are in high demand, but cannot  
17 yet be supplied from the Golgi complex. We provide evidence for Arp2/3 complex-dependent  
18 clathrin-mediated endocytosis of ciliary proteins, an increase in endocytic activity upon induction  
19 of ciliary growth, and relocalization of plasma membrane proteins to newly formed cilia. Our  
20 data support a new model of ciliary protein and membrane trafficking during early ciliogenesis  
21 whereby proteins previously targeted to the plasma membrane are reclaimed by Arp2/3  
22 complex-dependent clathrin-mediated endocytosis for initial ciliary assembly.  
23

## 24 INTRODUCTION

25 The cilium of the unicellular, green alga *Chlamydomonas reinhardtii* has long been used  
26 as a model due to its structural and mechanistic conservation relative to the cilia of mammalian  
27 cells. Cilia consist primarily of microtubules that extend from the surface of the cell and are  
28 ensheathed in plasma membrane. Their assembly relies on microtubule dynamics and  
29 trafficking of protein and membrane (Nachury, Seeley, and Jin 2010), as well as intraflagellar  
30 transport (IFT), a motor-based transport system that moves tubulin and other cargo from the  
31 base of the cilium to the tip and back again (Pedersen and Rosenbaum 2008).

32 Although cilia are composed of microtubules and depend on them for assembly, the  
33 mechanisms governing ciliary maintenance and assembly extend to other cytoskeletal  
34 components, namely actin. In fact, the microtubule organizing center of the cell, the centrosome,  
35 from which cilia are nucleated has been found to function as an actin organizer (Farina et al.  
36 2016; Inoue et al. 2019). In mammalian cells, cortical actin disruption results in increased ciliary  
37 length and percentage of ciliated cells (Kim et al. 2010; Park et al. 2008). Further, in mammalian  
38 cells, when ciliogenesis is triggered by serum starvation, preciliary vesicles are trafficked to the  
39 centriole where they fuse to form a ciliary vesicle around the budding cilium. In the intracellular  
40 pathway of ciliogenesis, it has been shown that when Arp2/3 complex-branched actin is lost,  
41 depletion of preciliary vesicles at the centriole occurs due to problems with vesicle fusion,  
42 suggesting a role for branched actin in intracellular ciliogenesis (Wu, Chen, and Tang 2018).  
43 Further, actin itself has even been found within cilia, suggesting that actin is a key protein  
44 involved in ciliary maintenance and assembly (Kiesel et al. 2020).

45 *Chlamydomonas* cells are ideal for tackling the question of actin-dependent ciliary  
46 trafficking due to their lack of a cortical actin network and their ability to undergo consistent and  
47 robust ciliogenesis without requiring serum starvation. In *Chlamydomonas*, disruption of actin  
48 networks with Cytochalasin D (CytoD) resulted in shorter steady-state cilia (W. L. Dentler and  
49 Adams 1992) and disruption with Latrunculin B (LatB), which sequesters monomers leading to  
50 eventual filament depolymerization, resulted in shortened cilia and impaired regeneration  
51 (Avasthi et al. 2014; Jack et al. 2019). *Chlamydomonas* actin networks are required for  
52 accumulation of IFT machinery at the base of cilia and for entry of IFT material into cilia (Avasthi  
53 et al. 2014), as well as for trafficking of post-Golgi vesicles to cilia, the synthesis of ciliary  
54 proteins, and the organization of the gating region at the base of cilia (Jack et al. 2019). Many  
55 key advances in our understanding of the relationship between cilia and actin have been  
56 discovered using *Chlamydomonas*, which is proving to be a useful model for studying the actin  
57 cytoskeleton and its ciliary functions.

58 The actin cytoskeleton of *Chlamydomonas* contains two actin genes: *IDA5*, a  
59 conventional actin with 91% sequence identity to human  $\beta$ -actin; and *NAP1*, a divergent actin  
60 that shares only 63% of its sequence with human  $\beta$ -actin (Hirono et al. 2003; Kato-Minoura et al.  
61 1998). We consider *NAP1* to be an actin-like protein as opposed to an actin related protein  
62 (ARP) because it has a higher sequence identity to actin than to conventional ARPs, and  
63 because it is able to functionally compensate for the conventional filamentous actin (Jack et al.  
64 2019; M. Onishi et al. 2018; M. Onishi, Pringle, and Cross 2016; Masayuki Onishi et al. 2019).  
65 Under normal, vegetative conditions, the conventional *IDA5* is the primary actin expressed, but  
66 when cells are treated with LatB, the LatB-insensitive *NAP1* is upregulated (M. Onishi et al.  
67 2018; M. Onishi, Pringle, and Cross 2016; Hirono et al. 2003). This separability of the two actins  
68 has led to the discovery that they can compensate for each other in ciliary maintenance and  
69 assembly (Jack et al. 2019). Studies of the role of actin in ciliary assembly have used global  
70 disruption by knocking out either one of the filamentous actins or acutely knocking out both, yet  
71 actin networks have diverse compositions and topologies that lead to specific subfunctions  
72 within cells.

73 Actin networks rely on the actin binding proteins that contribute to the formation,  
74 arrangement, and function of the network. One such actin binding protein is the Arp2/3 complex,

75 which nucleates branched or dendritic actin networks by nucleating a daughter filament off the  
76 side of an existing mother filament. The dendritic networks nucleated by the Arp2/3 complex are  
77 primarily found to be responsible for functions that involve membrane remodeling, for example  
78 lamellipodia and endocytosis (Campellone and Welch 2010). The Arp2/3 complex from most  
79 eukaryotes consists of seven subunits: Arp2, Arp3, and ARPC1-5 (**Supplemental Figure 1**) and  
80 each subunit plays a specific role of varying importance in the nucleation process. ARPC2 and  
81 ARPC4 form the core of the complex and the primary contacts with the mother filament, Arp2  
82 and Arp3 serve as the first subunits of the daughter filament, and ARPC1 and ARPC3 play a  
83 role in nucleation but are not critical for branch formation (Robinson et al. 2001; Gournier et al.  
84 2001). Each of these subunits are found in *Chlamydomonas* but have varying degrees of  
85 sequence homology compared with conventional Arp2/3 complexes (**Supplemental Figure 1**).  
86 Interestingly, the ARPC5 subunit has yet to be found in *Chlamydomonas*. ARPC5 is thought to  
87 be important for the association of ARPC1 to the complex, but a mammalian complex lacking  
88 ARPC5 and ARPC1 maintains some nucleating and branching activity and is able to cross-link  
89 actin normally (Gournier et al. 2001).

90 Here, using the chemical inhibitor CK-666 to inhibit the nucleating function of the Arp2/3  
91 complex (Hetrick et al. 2013) and a genetic mutant of a critical Arp2/3 complex member, ARPC4  
92 (Cheng et al. 2017; Li et al. 2019), we take a more delicate approach to investigating the role of  
93 actin in ciliary assembly by separating different actin networks into their subfunctions based on  
94 topology. Specifically, we probe the involvement of actin networks nucleated by the Arp2/3  
95 complex in ciliary maintenance and assembly. This approach in these cells has allowed us to  
96 propose a new model implicating a subset of filamentous actin in redistribution of membrane  
97 and proteins for the initial stages of ciliogenesis.

98  
99

## 100 RESULTS

101

### 102 **Loss of Arp2/3 complex function inhibits normal regeneration and maintenance of cilia:**

103 To answer questions involving the role of Arp2/3 complex-mediated actin networks in  
104 ciliary assembly, we primarily used two tools. First, we used the chemical inhibitor CK-666  
105 which blocks the nucleating ability of the Arp2/3 complex. Second, we obtained a null mutant of  
106 the critical Arp2/3 complex member, ARPC4 (Cheng et al. 2017; Li et al. 2019) from the  
107 *Chlamydomonas* Resource Center. This *arpc4* mutant was confirmed via PCR (**Supplemental**  
108 **Figure 2A**). We further evaluated this mutant by creating a genetic rescue where a V5-tagged  
109 ARPC4 construct is expressed in *arpc4* mutant cells, *arpc4:ARPC4-V5*. This was confirmed via  
110 PCR, western blot, and immunofluorescence (**Supplemental Figure 2**).

111 We first investigated the requirement for the Arp2/3 complex in maintenance of cilia by  
112 treating cells with varying concentrations of CK-666 or the inactive control CK-689 (250 $\mu$ M) for 2  
113 hours and measuring the effect on steady state ciliary length. Consistent with previous results  
114 (Avasthi et al. 2014), we found that treating cells with CK-666 decreased ciliary length,  
115 suggesting that the Arp2/3 complex is required for maintaining cilia (**Figure 1A**). We saw no  
116 changes in ciliary length with the inactive CK-689 (**Figure 1A**) or when *arpc4* mutant cells  
117 lacking a functional Arp2/3 complex were treated with CK-666 (**Supplemental Figure 3-4**).  
118 Untreated *arpc4* mutant cells did however recapitulate the CK-666 result by showing a  
119 decreased ciliary length when compared with wild-type cells (**Figure 1B**). This defect in ciliary  
120 length was not present in the rescue, *arpc4:ARPC4-V5* (**Figure 1B**). Overall, these results  
121 demonstrate through both chemical and genetic perturbation that the Arp2/3 complex is required  
122 for normal ciliary length maintenance.

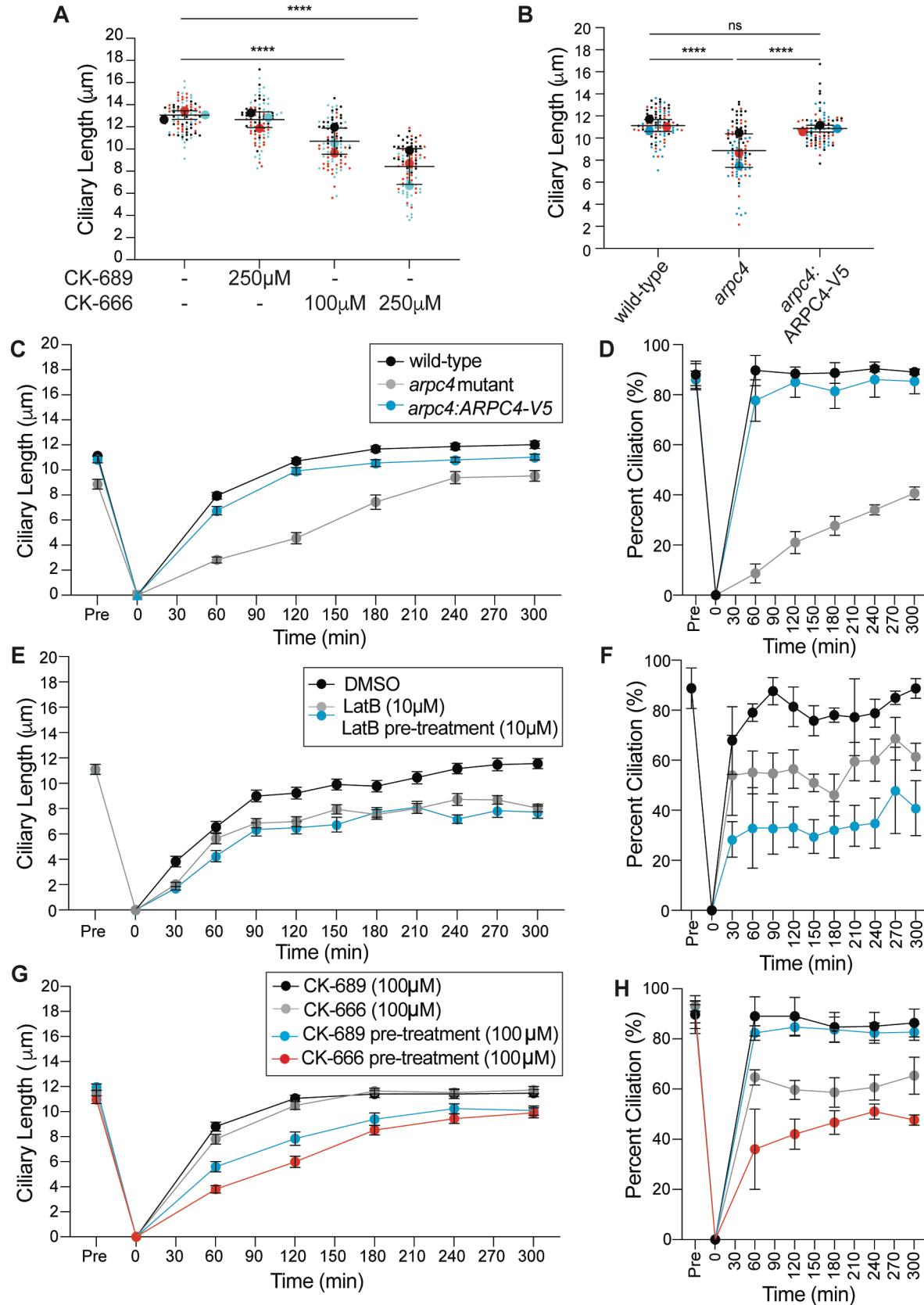
123 Next, we probed the involvement of Arp2/3 complex-nucleated actin in the more  
124 complicated process of ciliary assembly where there is a high demand for protein and  
125 membrane both from pools already existing in the cell and from synthesis (Wingfield et al. 2017;



126 Nachury, Seeley, and Jin 2010; Rohatgi and Snell 2010; Jack et al. 2019; Diener, Lupetti, and  
127 Rosenbaum 2015). Cells were deciliated by low pH shock and then allowed to synchronously  
128 regenerate cilia after being returned to normal pH (Paul A. Lefebvre 1995). We found that cells  
129 lacking a functional Arp2/3 complex were slow to regenerate their cilia, and two-thirds of cells  
130 did not regrow cilia at all (**Figure 1C**). This phenotype could be rescued by expression of  
131 ARPC4-V5 in the *arpc4* mutant (**Figure 1D**). Importantly, the most severe defect in assembly  
132 appeared to be in the initial steps when existing protein and membrane are being incorporated  
133 into cilia.

134 The striking decrease in ciliary assembly is puzzling because the loss of Arp2/3 complex  
135 function, and therefore only a subset of actin filaments, results in a more dramatic phenotype  
136 than that of the *nap1* mutants treated with LatB, which are lacking all filamentous actins (Jack et  
137 al. 2019). However, in the *arpc4* mutant cells, a functional Arp2/3 complex never exists, and  
138 therefore, cells never have Arp2/3 complex-mediated actin networks. In *nap1* mutant cells  
139 treated with LatB, the treatment begins shortly after deciliation resulting in an acute perturbation.  
140 Further, LatB functions by sequestering actin monomers to promote filament disassembly, and  
141 thus the effects may not be immediate (Spector et al. 1989). Therefore, it is likely that there is a  
142 brief window where actin filaments can assert their initial role in ciliary regeneration before being  
143 depolymerized. To avoid this, we began the LatB treatment in *nap1* mutants 30 minutes before  
144 deciliation. This pre-treatment allows us to observe what happens when actin is not present  
145 immediately after deciliation. (**Figure 1E-F**). In this case, we see slightly decreased ciliary length  
146 consistent with the acute treatment but dramatically decreased percent ciliation, which is  
147 consistent with the *arpc4* mutant results.

148 This can also be observed with the inhibitor of the Arp2/3 complex, CK-666. In cells  
149 treated with CK-666 immediately following deciliation, there is likely a window where the Arp2/3  
150 complex can assert its role in assembly before being inhibited by CK-666. By pre-treating cells  
151 with CK-666 for 1 hour before deciliation, we are able to observe what happens in the absence  
152 of Arp2/3 complex function immediately following deciliation. When we do so, we see a more  
153 dramatic defect in both ciliary length and percent ciliation than we do with just acute CK-666  
154 treatment (**Figure 1G-H**), suggesting that the Arp2/3 complex is required for some very early  
155 initial step of ciliary assembly that occurs even before we have a chance to treat the cells.  
156



157  
158  
159

**Figure 1. The Arp2/3 complex is required for normal ciliary maintenance and assembly.** **A)** Wild-type cells containing a full active Arp2/3 complex were treated with 100  $\mu\text{M}$  or 250  $\mu\text{M}$  CK-666 or the inactive CK-689 for 2 hours.

160 Cells were then imaged using a DIC microscope and cilia were measure in ImageJ. Superplots are used to show the  
161 mean of 3 separate experiments with error bars representing standard deviation. n=30 for each treatment in 3 separate  
162 experiments. P<0.0001. **B)** Wild-type cells, *arpc4* mutant cells, and *arpc4* mutant cells expressing *ARPC4-V5* steady  
163 state cilia were also measured with no treatment. Superplots are used to show the mean of 3 separate experiments  
164 with error bars representing standard deviation. n=30 for each strain for 3 separate experiments. P<0.0001. **C)** Wild-  
165 type cells and *arpc4* mutant cells were deciliated using a pH shock and then cilia were allowed to regrow. The black  
166 line represents wild-type, while the grey line represents the *arpc4* mutant. The numbers above or below each point  
167 show the percent ciliation for the wild-type and *arpc4* mutant cells respectively. Means are displayed with error bars  
168 representing 95% confidence interval. n=30 for each strain and each time point in 3 separate experiments. For every  
169 time point except 0 min, P<0.0001 in terms of both length and percent ciliation. **D)** Wild-type cells, *arpc4* mutant cells,  
170 and *arpc4* mutant cells expressing *ARPC4-V5* were deciliated using a pH shock and then allowed to regrow. The black  
171 line represents wild-type, while the grey line represents the *arpc4* mutant and the cyan line represent the *arpc4* mutant  
172 expressing *ARPC4-V5*. Means are displayed with error bars representing 95% confidence interval. n=30 for each strain  
173 and each time point in 3 separate experiments. **E)** *nap1* mutant cells were pre-treated with 10 $\mu$ M LatB for 30 minutes  
174 before deciliation or treated with LatB upon the return to neutral pH following deciliation. The black line represents  
175 untreated cells, while the light grey line represents cells treated with LatB following deciliation and the dark grey line  
176 represents cells pre-treated with LatB. Error bars represent 95% confidence interval. n=30 for 3 separate experiments.  
177 For every time point P>0.0001 between DMSO and treated samples, except 30min (10 $\mu$ M LatB) which is ns. **F)** Percent  
178 ciliation for the experiment in D. Line color is the same as D. Error bars represent standard deviation. **G)** Wild-type cells  
179 were pre-treated with CK-666 or the inactive CK-689 (100 $\mu$ M) for 1 hour before deciliation of treated with CK-666 or the  
180 inactive CK-689 (100 $\mu$ M) following deciliation. Error bars represent 95% confidence interval. n=30 for 3 separate  
181 experiments. **H)** Percent ciliation for the experiments in G. Error bars represent standard deviation. n=100 in 3 separate  
182 experiments.  
183

184

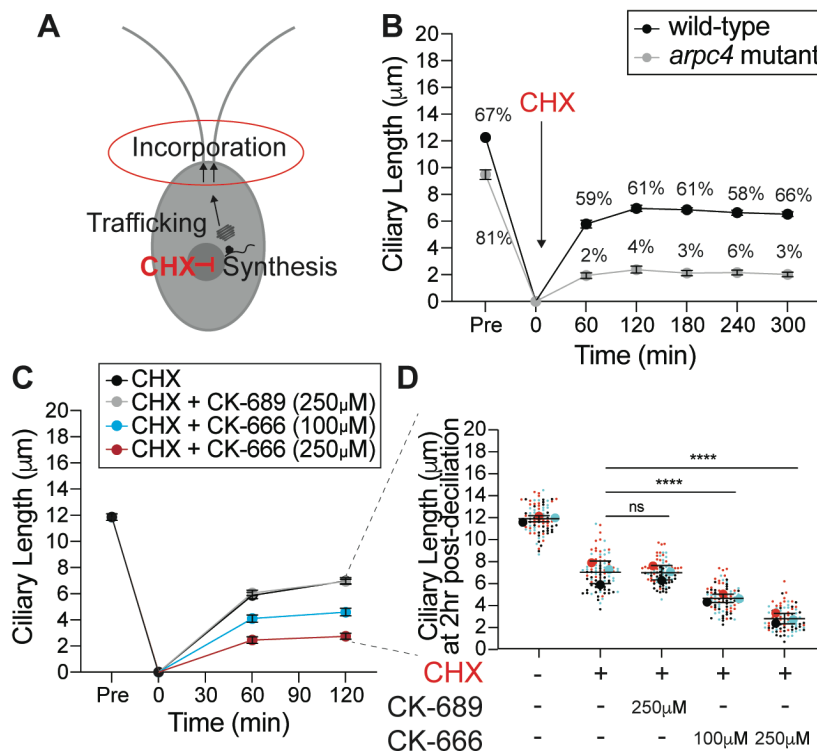
### 185 **The Arp2/3 complex is required for the incorporation of existing membrane and proteins** 186 **for ciliary assembly:**

187 There are several distinct, filamentous actin-dependent steps of ciliary assembly after  
188 severing, including the incorporation of existing protein and membrane and the synthesis of new  
189 protein for cilia. Using a method that labels nascent peptides, we found that loss of ARPC4 did  
190 not prevent upregulation of translation following deciliation (**Supplemental Figure 5**). In this  
191 experiment, we are halting translation and fluorescently labelling newly translated polypeptides.  
192 Wild-type and *arpc4* mutant cells were tested using this reaction either before deciliation,  
193 following deciliation and one hour of regrowth, or following deciliation and one hour of regrowth  
194 in cycloheximide (CHX), which blocks protein synthesis by blocking the elongation step of  
195 protein translation. Both wild-type and *arpc4* mutant cells displayed an increase in cell  
196 fluorescence, especially in the area around the nucleus, following deciliation, indicating an  
197 increase in protein synthesis following deciliation (**Supplemental Figure 5**). Importantly, this  
198 increase in cell fluorescence was not significantly different between wild-type and *arpc4* mutant  
199 cells, suggesting that the loss of Arp2/3 complex function does not prevent the upregulation of  
200 protein synthesis that follows deciliation. This also suggests that the cells are aware that the  
201 cilia have been severed, as they respond with increased protein synthesis.

202 Given that *arpc4* mutant cells respond to deciliation with protein synthesis, another  
203 possibility for the role of the Arp2/3 complex in ciliary assembly involves the first step, which  
204 requires that a pool of existing proteins and membrane are incorporated into cilia in an actin-  
205 dependent manner (Jack et al. 2019). Further, disruption of Arp2/3 complex-mediated actin  
206 networks results in slow initial ciliary assembly, when it is likely that existing protein is being  
207 incorporated. We tested this by treating cells with cycloheximide (CHX), a protein synthesis  
208 inhibitor, we can eliminate the contribution of two steps in the process of ciliary assembly  
209 (**Figure 2A, Supplemental Figure 4**) (Rosenbaum, Moulder, and Ringo 1969). Without protein  
210 synthesis, there is no trafficking or incorporation of new proteins. Therefore, any ciliary growth  
211 we see is due to the incorporation of the existing protein alone. Under normal conditions, cells  
212 that are deciliated and treated with cycloheximide typically grow cilia to about half-length, or  
213 6 $\mu$ m, within 2 hours (**Figure 2B**). In the *arpc4* mutant strain treated with CK-666, cilia display  
214 minimal growth (**Figure 2B**). In fact, throughout a five-hour period, only 6% of cells were able to

215 form cilia at all (**Figure 2B**). This suggests that the Arp2/3 complex and the actin networks  
 216 nucleated by the complex are indispensable for the incorporation of existing protein and  
 217 membrane during ciliary assembly.

218 We suspected that the *arpc4* mutant cells either lacked the normal pool of ciliary  
 219 precursor proteins or were unable to incorporate it. However, the inability of the genetic mutants  
 220 to regenerate in cycloheximide prevents us from being able to do the typical studies testing new  
 221 protein synthesis, precursor pool size, and new protein incorporation outlined in Jack et al. 2018  
 222 as they all require regeneration in cycloheximide. To get around this, we used an acute  
 223 perturbation through chemical inhibition in wild-type cells that have a normal ciliary precursor  
 224 pool (as evidenced by their ability to grow to half-length in cycloheximide). These cells were  
 225 deciliated and then CK-666 was added (in addition to cycloheximide) only for the regrowth, and  
 226 thus it was not able to affect the size of the precursor pool. Cells treated with CK-666 and  
 227 cycloheximide could not incorporate the precursor pool we know exists in these wild-type cells  
 228 into cilia, while cilia of cells treated with only cycloheximide or cycloheximide and the inactive  
 229 control for CK-666, CK-689 were able to grow to half length (**Figure 2C-D, Supplemental**  
 230 **Figure 4**). This suggests that the problem with incorporation we see in cells lacking a functional  
 231 Arp2/3 complex lies outside of the availability of the precursor pool.  
 232



233 **Figure 2. The Arp2/3 complex is required for incorporation of existing protein during ciliary assembly. A)**  
 234 Treating cells with cycloheximide inhibits protein synthesis, which means only incorporation of existing protein into the  
 235 cilia is observed. **B)** Wild-type cells and *arpc4* mutants were deciliated and then allowed to regrow in 10μM CHX. The  
 236 percentages above the lines represent the percent of cells with cilia at the indicated time points. The mean is shown  
 237 with error bars representing 95% confidence interval. n=30 for each strain and each time point in 3 separate  
 238 experiments. For every time point besides 0 min, P<0.0001 for both length and percent ciliation. **C)** Wild-type cells  
 239 were deciliated and then treated with a combination of 10μM cycloheximide (CHX) and CK-666 (100μM or 250μM) or  
 240 CK-689 (the inactive control, 250μM) at the same concentration during regrowth. The mean is shown with error bars  
 241 representing 95% confidence interval. n=30 for each strain and each time point in 3 separate experiments. At both 1  
 242 and 2 hour time points P<0.0001 for cells treated with CK-666 compared to wild-type cells, and ns for cells treated  
 243 with CK-689 compared to wild-type cells. **D)** The graph shows the 2 hour time point from C, or the length of their cilia  
 244 after 2 hours of treatment and regrowth. Superplots are used to show the mean of 3 separate experiments with error  
 245

246 bars representing standard deviation. n=30 for each treatment group 3 separate experiments. For both the 100 $\mu$ M  
247 and 250 $\mu$ M CK-666 treatments with CHX, P<0.0001.

248  
249

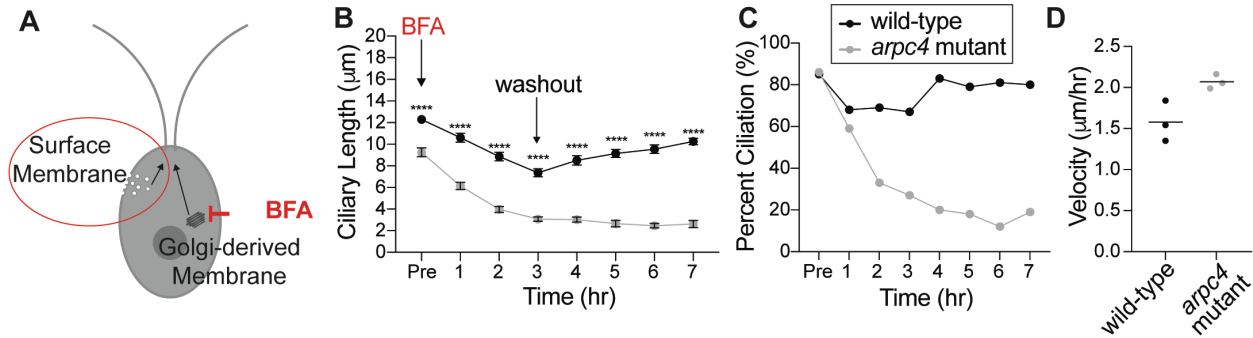
### 250 **Cilia of *arpc4* mutant cells resorb faster in the absence of the Golgi:**

251 Because we see defects in ciliary assembly and maintenance when cells are likely  
252 incorporating existing protein, and we know the protein needed for assembly is in excess due to  
253 our acute perturbations with CK-666, we next investigated membrane delivery to cilia. This is of  
254 particular interest as the Arp2/3 complex is canonically thought to be involved in membrane  
255 remodeling functions. Typically, the Golgi is thought to be the main source of membrane for cilia  
256 (Nachury, Seeley, and Jin 2010; Rohatgi and Snell 2010), and both ciliary membrane,  
257 membrane proteins, and even axonemal proteins are transported in or attached to vesicles in  
258 cytosol (Wood and Rosenbaum 2014). In *Chlamydomonas*, this has been demonstrated by the  
259 ciliary shortening of cells treated with Brefeldin A (BFA), a drug that causes Golgi collapse by  
260 interfering with ER to Golgi transport (W. Dentler 2013). To determine if the Arp2/3 complex is  
261 involved in the trafficking of new protein from the Golgi to cilia, we examined the Golgi following  
262 deciliation using transmission electron microscopy (TEM) in *arpc4* mutants (**Supplemental**  
263 **Figure 6A**). The Golgi appeared grossly normal, and in all cases had approximately the same  
264 number of cisternae (**Supplemental Figure 6A-B**) and did not show an abnormal accumulation  
265 of post-Golgi membrane as previously reported when perturbing all filamentous actin (Jack et  
266 al., 2019).

267 Alternative pathways for delivery of material to the cilia have also been found in  
268 *Chlamydomonas*. For example, surface proteins were biotinylated and then cells were  
269 deciliated, meaning the membrane and proteins within cilia were lost. When cilia were allowed  
270 to regrow, biotinylated proteins were found to reside within the new cilia suggesting they came  
271 from the plasma membrane (W. Dentler 2013). Therefore, we hypothesized that due to its role  
272 in membrane remodeling, and particularly endocytosis, in other organisms, the Arp2/3 complex  
273 may be part of an endocytic pathway that provides membrane and perhaps membrane proteins  
274 to cilia (**Figure 3A**). To test if membrane could be coming from an endosomal or endocytic  
275 source other than the Golgi, we treated cells with 36 $\mu$ M BFA to collapse the Golgi and block  
276 exocytosis so cells would be forced to utilize other sources of ciliary proteins and membranes.  
277 Wild-type cilia treated with BFA resorb slowly, but *arpc4* mutant cells had a faster resorption  
278 rate (**Figure 3B and D, Supplemental Figure 4**). Further, the number of cells with cilia in the  
279 *arpc4* mutant cells dramatically decreased with BFA treatment (**Figure 3C**). Meanwhile, cells  
280 treated with other known ciliary resorption-inducing drugs that do not specifically target Golgi  
281 traffic, 3-isobutyl-1-methylxanthine (IBMX) (Pasquale and Goodenough 1987) or sodium  
282 pyrophosphate (NaPPi) (P. A. Lefebvre et al. 1978) show an increased velocity of resorption in  
283 the wild-type cells compared to the *arpc4* mutant cells (**Supplemental Figure 7**), suggesting the  
284 faster resorption of the *arpc4* mutant cells in BFA is specific to the effects of BFA on the cell.  
285 Thus, wild-type cells are more capable of maintaining cilia without membrane supply from the  
286 Golgi, suggesting that there must be another source for membrane that is dependent upon the  
287 Arp2/3 complex.

288





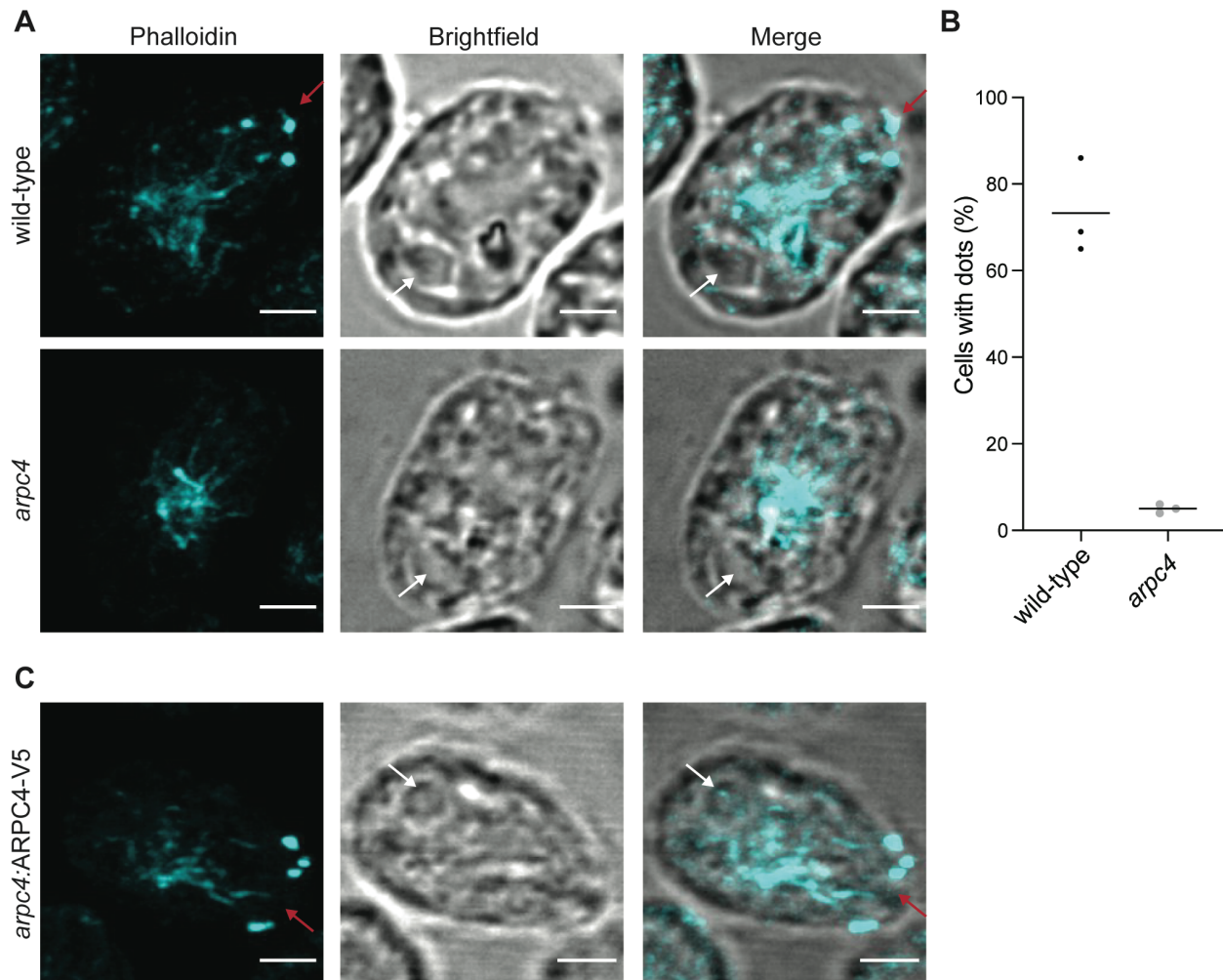
289  
290  
291  
292  
293  
294  
295  
296  
297  
298  
299

**Figure 3. The Arp2/3 complex is required for ciliary maintenance in the absence of intact Golgi. A)** Treating cells with Brefeldin A (BFA) causes the Golgi to collapse meaning any membranes and proteins used to maintain the cilia must come from other sources. **B)** Cells were treated with  $36\mu\text{M}$  BFA for 3 hours at which time the drug was washed out. Wild-type is represented by black, while *arpc4* mutants are grey. The mean is shown with error bars representing 95% confidence interval. Error bars represent 95% confidence interval of the mean.  $n=30$  for each time point and each strain in 3 separate experiments. \*\*\*\* represents  $P<0.0001$ . **C)** Percent ciliation of the cells in B.  $n=100$ . **D)** Resorption speed for wild-type cells and *arpc4* mutant cells as determined by fitting a line to the first 4 time points before washout and determining the slope of the line. Line represents the mean of 3 separate experiments.  $N=3$ .  $P=0.0314$

### 300 Apical actin dots are dependent on the Arp2/3 complex:

301 Since ciliary membrane proteins can come from the Golgi or the plasma membrane and  
302 *arpc4* mutant cells have a more severe defect in incorporating ciliary proteins from non-Golgi  
303 sources, we asked if Arp2/3 complex-mediated actin networks might be responsible for  
304 endocytosis from the plasma membrane in *Chlamydomonas* as it is in other organisms. To  
305 determine where in the cell Arp2/3 complex-mediated actin networks might be acting, we looked  
306 directly at the effects of loss of Arp2/3 complex function on the actin structures in the cell. Using  
307 new protocols for the visualization of actin in *Chlamydomonas* developed by our lab (Craig et al.  
308 2019), we stained wild-type cells and *arpc4* mutant cells with fluorescent phalloidin. In wild-type  
309 cells, apical dots reminiscent of endocytic actin patches in yeast are typically seen near the  
310 base of cilia (**Figure 4A**). We quantified the presence of these dots in the wild-type cells  
311 compared to the *arpc4* mutant cells (**Figure 4A-B**). We found that while about 70% of wild-type  
312 cells contain the dots, only about 5% of the *arpc4* mutant cells had dots (**Figure 4B**), suggesting  
313 the Arp2/3 complex is required for the formation of this actin structure. This phenotype was  
314 rescued by the expression of the ARPC4-V5 construct in the *arpc4* mutant cells (**Figure 4C**).  
315 The reliance of this structure on the Arp2/3 complex, led us to further question whether these  
316 dots could represent endocytic membrane remodeling.

317



318  
319 **Figure 4. Loss of a functional Arp2/3 complex results in changes in actin distribution.** **A)** Wild-type and *arpc4*  
320 mutant cells stained with phalloidin to visualize the actin network along with brightfield to show cell orientation. Images  
321 were taken as a z-stack using airsycan imaging and are shown as a maximum intensity projection. Red arrow is pointing  
322 to dots at the apex of the cell, and white arrow is pointing to the pyrenoid near the basal end of the cell. Scale bars  
323 represent 2 $\mu$ m. **B)** Percentage of cells with apical dots as shown in A. Percentages taken from 3 separate experiments  
324 where n=100. Line represents the mean.  $P < 0.0001$ . **C)** Presence of apical dots in the *arpc4* mutant rescue expressing  
325 ARPC4-V5. Images were taken as a z-stack using airsycan imaging and are shown as a maximum intensity projection.  
326 Red arrow is pointing to dots at the apex of the cell, and white arrow is pointing to the pyrenoid near the basal end of  
327 the cell. Scale bars represent 2 $\mu$ m.

328  
329

### 330 **Endocytosis in *Chlamydomonas* is likely clathrin-dependent:**

331 The Arp2/3 complex is conventionally thought to be involved in endocytosis in cell-walled  
332 yeast to overcome turgor pressure (Aghamohammadzadeh and Ayscough 2009; Basu,  
333 Munteanu, and Chang 2014; Carlsson and Bayly 2014). *Chlamydomonas* cells also have a cell  
334 wall and since the apical actin dots resemble these endocytic pits (Goode, Eskin, and Wendland  
335 2015; Adams and Pringle 1984; Ayscough et al. 1997), we hypothesized that Arp2/3 complex  
336 and actin-dependent endocytosis might be occurring in *Chlamydomonas* even though this  
337 process has not yet been directly demonstrated in this organism. To determine what kind of  
338 endocytosis was likely occurring in these cells, we compared the endocytosis-related proteins  
339 found in mammals and plants to those in *Chlamydomonas* (**Figure 5A**). We found that  
340 *Chlamydomonas* lacks much of the important machinery for almost all typical endocytosis  
341 processes, including caveolin for caveolin-mediated endocytosis, flotillin for flotillin-dependent



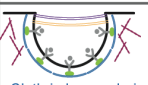
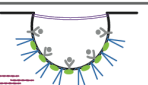
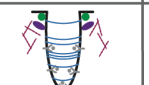
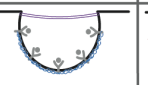
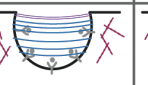

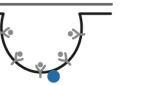
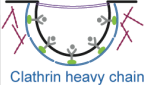




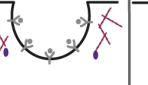




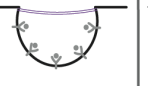
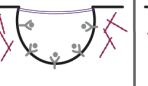


342 endocytosis, and endophilin for endophilin-dependent endocytosis (**Figure 5A**). However, most  
343 of the canonical clathrin-related endocytosis machinery could be found in *Chlamydomonas*, and  
344 thus, clathrin-mediated endocytosis is conserved to a higher extent than other endocytic  
345 mechanisms.

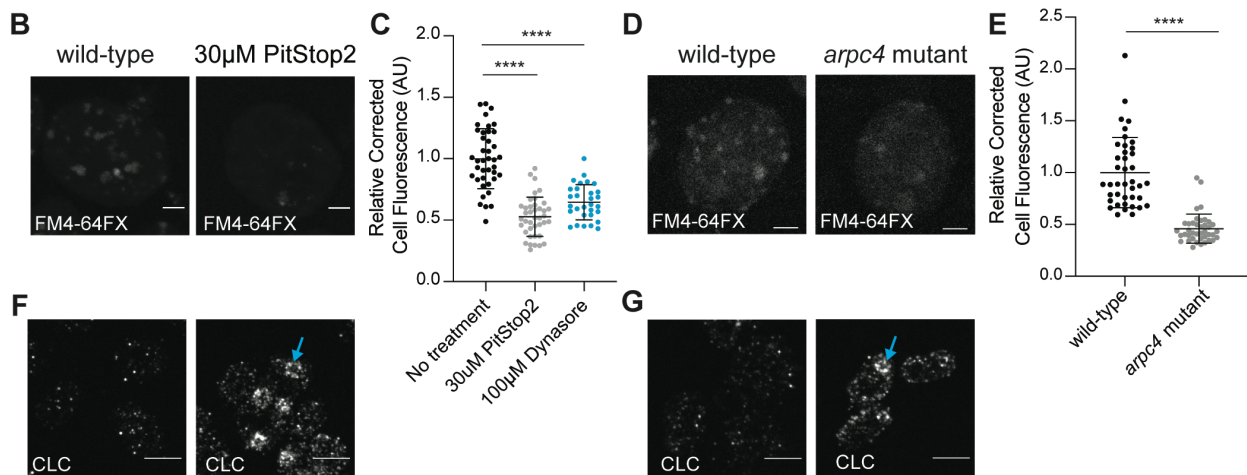
346 We aimed to further probe the likelihood of clathrin-mediated endocytosis occurring in  
347 *Chlamydomonas*. However, a mutant for the proteins involved in clathrin-mediated endocytosis  
348 does not currently exist and methods of targeted mutagenesis in *Chlamydomonas* are not yet  
349 reliable. Therefore, we turned to our best alternative PitStop2, which inhibits the interaction of  
350 adaptor proteins with clathrin, halting clathrin endocytosis, despite the reported off-target effects  
351 on global endocytosis in mammalian cells (Willox, Sahraoui, and Royle 2014) (**Supplemental**  
352 **Figure 4**). Additionally, we used the dynamin inhibitor Dynasore, which is also thought to block  
353 endocytosis by inhibiting the GTPase activity of dynamin (Macia et al. 2006). For this  
354 experiment, we used the fixable lipophilic dye FM 4-64FX (Cochilla, Angleson, and Betz 1999;  
355 Gachet and Hyams 2005) (Thermo Scientific). This dye is impermeable to the plasma  
356 membrane but is usually quickly endocytosed into cells showing bright foci where dye is  
357 enriched in endocytosed compartments. Thus, we incubated the dye for only 1 minute to allow  
358 enough time for internalization into endosomes but not enough for incorporation into various  
359 cellular membrane structures. The ability of PitStop2-treated cells to internalize membrane was  
360 measured by calculating the total cell fluorescence inside the cell after allowing dye to be  
361 internalized (**Figure 5B**). We found that cells treated with 30 $\mu$ M PitStop2 or 100 $\mu$ M Dynasore  
362 have significantly decreased membrane internalization (**Figure 5C**), which further supports the  
363 idea that endocytosis of some kind is occurring in these cells and that it is likely clathrin-  
364 mediated.

365 Next, we tested whether the endocytosis is Arp2/3 complex-dependent by using this  
366 membrane internalization assay on *arpc4* mutant cells compared to wild-type cells. We found  
367 that cells lacking a functional Arp2/3 complex have decreased total cell fluorescence (**Figure**  
368 **5D-E**) suggesting the endocytosis in *Chlamydomonas* is Arp2/3 complex-dependent.

369 To better demonstrate the relationship between the Arp2/3 complex and endocytosis, we  
370 used a clathrin light chain antibody to stain cells. In both PitStop2 treated cells and *arpc4* mutant  
371 cells, but not in untreated wild-type cells, we see a mislocalization of clathrin staining around the  
372 pyrenoid (**Supplemental Figure 8, Figure 5F-G**). Although the reason for this accumulation of  
373 clathrin around the pyrenoid is not clear, the interesting takeaway from this data is that  
374 disruption of either endocytosis with PitStop2 or of Arp2/3 function results in defects in  
375 membrane internalization and clathrin localization. These data support a role for the Arp2/3  
376 complex in endocytosis in *Chlamydomonas*.

377

<b>A</b>	Clathrin	Caveolin	CLIC/GEEC	Flotillin	Fast endophilin	IL2RB	Arf6
<b>Animals</b> ( <i>Homo sapiens</i> )	 <ul style="list-style-type: none"> <li>Clathrin heavy chain</li> <li>Clathrin light chain</li> <li>AP2 proteins</li> <li>Dynamin</li> <li>Actin + ABPs</li> <li>F-BAR</li> <li>Rab5</li> <li>Arf6</li> <li>Epsin</li> </ul>	 <ul style="list-style-type: none"> <li>Caveolin</li> <li>Cav1</li> <li>Dynamin</li> <li>Actin + ABPs</li> <li>PKC</li> <li>Syntaxin-6</li> </ul>	 <ul style="list-style-type: none"> <li>GRAF1</li> <li>Cdc42</li> <li>Arf1</li> <li>Actin + ABPs</li> </ul>	 <ul style="list-style-type: none"> <li>Flotillin</li> <li>Dynamin</li> <li>MAPK pathway</li> <li>Src</li> <li>Fyn kinase</li> </ul>	 <ul style="list-style-type: none"> <li>Endophilin</li> <li>Dynamin</li> <li>Actin + ABP</li> <li>WASP</li> </ul>	 <ul style="list-style-type: none"> <li>WAVE</li> <li>Rac1</li> <li>PAK1/2</li> <li>PI3K</li> <li>Actin + ABPs</li> <li>RhoA</li> <li>Vav2</li> </ul>	 <ul style="list-style-type: none"> <li>Arf6</li> <li>CD59</li> <li>CarboxypeptidaseE</li> <li>PhospholipaseD</li> </ul>
<b>Plants</b> ( <i>Arabidopsis thaliana</i> )	 <ul style="list-style-type: none"> <li>Clathrin heavy chain</li> <li>Clathrin light chain</li> <li>AP2 proteins</li> <li>Dynamin</li> <li>Actin + ABPs</li> <li>Rab5</li> <li>Arf6</li> <li>Epsin</li> <li>Missing: F-BAR</li> </ul>	 <ul style="list-style-type: none"> <li>Dynamin</li> <li>Actin + ABPs</li> <li>PKC</li> <li>Syntaxin-6</li> <li>Missing: Caveolin</li> <li>Cav1</li> </ul>	 <ul style="list-style-type: none"> <li>Cdc42</li> <li>Arf1</li> <li>Actin + ABPs</li> <li>Missing: GRAF1</li> </ul>	 <ul style="list-style-type: none"> <li>Dynamin</li> <li>MAPK pathway</li> <li>Src</li> <li>Fyn kinase</li> <li>Missing: Flotillin</li> </ul>	 <ul style="list-style-type: none"> <li>Dynamin</li> <li>Actin + ABP</li> <li>Missing: Endophilin</li> <li>WASP</li> </ul>	 <ul style="list-style-type: none"> <li>Rac1</li> <li>Actin + ABPs</li> <li>RhoA</li> <li>Missing: WAVE</li> <li>PAK1/2</li> <li>Vav2</li> <li>PI3K</li> </ul>	 <ul style="list-style-type: none"> <li>Arf6</li> <li>CarboxypeptidaseE</li> <li>Missing: CD59</li> <li>PhospholipaseD</li> </ul>
<b><i>Chlamydomonas reinhardtii</i></b>	 <ul style="list-style-type: none"> <li>Clathrin heavy chain</li> <li>Clathrin light chain</li> <li>AP2 proteins</li> <li>Dynamin</li> <li>Actin + ABPs</li> <li>Rab5</li> <li>Arf6</li> <li>Epsin</li> <li>Missing: F-BAR</li> </ul>	 <ul style="list-style-type: none"> <li>Dynamin</li> <li>Actin + ABPs</li> <li>PKC</li> <li>Syntaxin-6</li> <li>Missing: Caveolin</li> <li>Cav1</li> </ul>	 <ul style="list-style-type: none"> <li>Cdc42</li> <li>Arf1</li> <li>Actin + ABPs</li> <li>Missing: GRAF1</li> </ul>	 <ul style="list-style-type: none"> <li>Dynamin</li> <li>MAPK pathway</li> <li>Src</li> <li>Fyn kinase</li> <li>Missing: Flotillin</li> </ul>	 <ul style="list-style-type: none"> <li>Dynamin</li> <li>Actin + ABP</li> <li>Missing: Endophilin</li> <li>WASP</li> </ul>	 <ul style="list-style-type: none"> <li>Rac1</li> <li>Actin + ABPs</li> <li>RhoA</li> <li>Missing: WAVE</li> <li>PAK1/2</li> <li>Vav2</li> <li>PI3K</li> </ul>	 <ul style="list-style-type: none"> <li>Arf6</li> <li>CarboxypeptidaseE</li> <li>Missing: CD59</li> <li>PhospholipaseD</li> </ul>



**Figure 5. Arp2/3 complex-dependent endocytosis is conserved in *Chlamydomonas*.** **A)** Gene presence was determined using BLAST. Word colors correspond to diagram colors. **B)** Cells treated with 30µM PitStop2 were incubated with FM4-64FX and imaged on a spinning disk confocal. Max intensity projections of z-stacks are shown. Scale bars are 2µm. **C)** The background corrected fluorescence for each sample, including cells treated with 100µM Dynasore. The mean is shown with error bars showing standard deviation. n=30 in 3 separate experiments. P<0.0001. **D)** Wild-type and *arpc4* mutant cells treated with FM4-64FX and imaged on a spinning disk confocal. Max intensity projections of z-stacks are shown. Scale bars are 2µm. **E)** The background corrected fluorescence for each sample. The mean is shown with error bars representing standard deviation. n=30 in 3 separate experiments. P<0.0001. **F)** Wild-type and PitStop2 treated cells, and *arpc4* mutant cells were stained with clathrin light chain antibody and imaged using a spinning disk confocal. Cyan arrows point to accumulation around the pyrenoid. Scale bar represents 5µm. **G)** Wild-type and *arpc4* mutant cells were stained with clathrin light chain antibody and imaged using a spinning disk confocal. Cyan arrows point to accumulation around the pyrenoid. Scale bar represents 5µm.

378  
379  
380  
381  
382  
383  
384  
385  
386  
387  
388  
389  
390  
391  
392

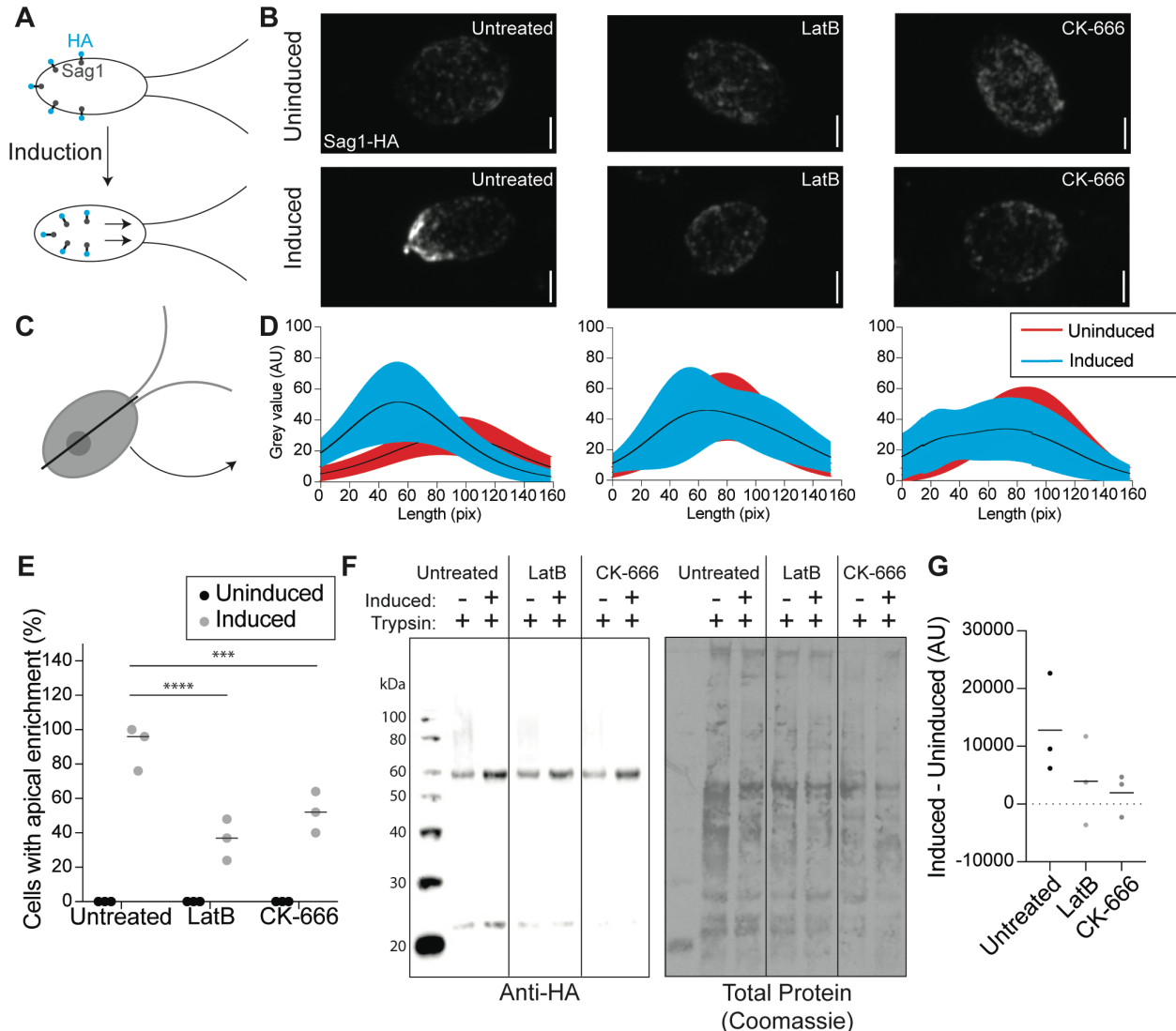
393 **The Arp2/3 complex is required for the internalization and relocalization of a membrane**  
394 **protein from the periphery of the cell to cilia:**

395       Upon finding that there is likely Arp2/3 complex-dependent clathrin-mediated  
396 endocytosis in *Chlamydomonas*, we next asked if this endocytosis could be responsible for the  
397 relocalization and internalization of a known ciliary protein. SAG1 is a membrane protein that is  
398 important for mating in *Chlamydomonas* cells (Belzile et al. 2013; Ranjan, Awasthi, and Snell  
399 2019). When cells are induced for mating with dibutyryl-cAMP (db-cAMP), SAG1 must relocalize  
400 from the cell periphery to cilia, where it facilitates ciliary adhesion between mating cells. This  
401 relocalization of SAG1 is thought to occur through internalization of the protein followed by  
402 internal trafficking on microtubules to the base of cilia (Belzile et al. 2013; Ranjan, Awasthi, and  
403 Snell 2019).

404       We examined whether actin and the Arp2/3 complex were required for the transport of  
405 HA-tagged SAG1 to the apex of the cell and cilia for agglutination during mating (**Figure 6A**).  
406 Using immunofluorescence, we observed cells treated with either 10 $\mu$ M LatB to depolymerize  
407 IDA5 or 250 $\mu$ M CK-666 to perturb the Arp2/3 complex (**Figure 6, Supplemental Figure 4**).  
408 Before induction, SAG1-HA localized to the periphery of the cell (**Figure 6B, top**). 30 minutes  
409 after induction with db-cAMP, SAG1-HA relocalized to the apex of the cell and to cilia in  
410 untreated cells (**Figure 6B, left**). In both LatB and CK-666 treated cells, this apical enrichment  
411 was greatly decreased (**Figure 6B, middle and right**). To quantify this, line scans were drawn  
412 through the cell from the apex to the basal region (**Figure 6C-D**). The percentage of cells with  
413 apical enrichment was calculated, and it was found that untreated cells had a higher percent of  
414 apical enrichment when compared with LatB or CK-666 treated cells (**Figure 6E**). Thus, cells  
415 with perturbed Arp2/3 complex-mediated filamentous actin show decreased efficiency of SAG1-  
416 HA relocalization.

417       We next asked if this decrease in relocalization in cells with actin and Arp2/3 complex  
418 inhibition could be due to a decrease in the internalization of SAG1-HA through a process that  
419 seems to require endocytosis. To investigate this, we used a method first described by Belzile et  
420 al. 2013, where cells were induced and treated with a low percentage (0.01%) of trypsin, which  
421 will hydrolyze exterior proteins but cannot enter the cell. In untreated cells, we see an increase  
422 in SAG1-HA protein levels following induction because SAG1-HA is internalized and becomes  
423 protected from trypsin (**Figure 6F**). In cells treated with either 10 $\mu$ M LatB or 250 $\mu$ M CK-666 we  
424 see a decrease in this trypsin protection as shown in the western blot (**Figure 6F**). This was  
425 further quantified by subtracting the amount of protein before induction from the amount of  
426 protein present after induction, which gives a value representing the amount of SAG1-HA  
427 protected from trypsin due to internalization in these cells (**Figure 6G**). The decrease in SAG1-  
428 HA following induction in cells with decreased filamentous actin and Arp2/3 complex function  
429 indicates a role for Arp2/3 complex-mediated actin networks in internalization of this specific  
430 ciliary membrane protein.

431



432  
 433 **Figure 6. The Arp2/3 complex is required for the relocalization and internalization of the ciliary protein SAG1**  
 434 **for mating. A)** When mating is induced SAG1-HA is internalized and relocalized to the apex of the cells and cilia for  
 435 agglutination. **B)** Maximum intensity projections of z-stacks taken using spinning disk confocal microscopy of SAG1-  
 436 HA. Left is untreated, middle is treated with 10  $\mu$ M LatB, and right is treated with 250  $\mu$ M CK-666. Top row of images  
 437 are uninduced and bottom row of images are induced with db-cAMP. Scale bar represents 2  $\mu$ m. **C)** Diagram  
 438 representing line scans taken through the cells in z-stack sum images. **D)** Line scans were taken from the apex of the  
 439 cell to the basal region of the cell in untreated cells (left), LatB treated cells (middle), and CK-666 (right). Lines scans  
 440 were normalized and fit with a gaussian curve. The curves were averaged. Black lines represent mean and then shaded  
 441 regions represent standard deviation. Grey represents uninduced samples, green represent induced samples. 0 on the  
 442 y-axis represents the apical region of the cell. n=30 from a single representative experiment. **E)** Percentage of cells  
 443 with apical enrichment based on E for uninduced (black) and induced (grey) cells for each treatment group. The mean  
 444 is shown with error bars representing standard deviation. n=30 for 3 separate experiments for each treatment. **F)**  
 445 Western blot showing amount of SAG1-HA in uninduced and induced cells in each treatment group all treated with  
 446 0.01% trypsin. **G)** Intensity of the bands in H were normalized to the total protein as determined by amido black staining  
 447 and quantified in ImageJ was used to subtract uninduced from induced to give a representation of the amount of SAG1-  
 448 HA internalized with induction. Line represents mean of 3 separate experiments.

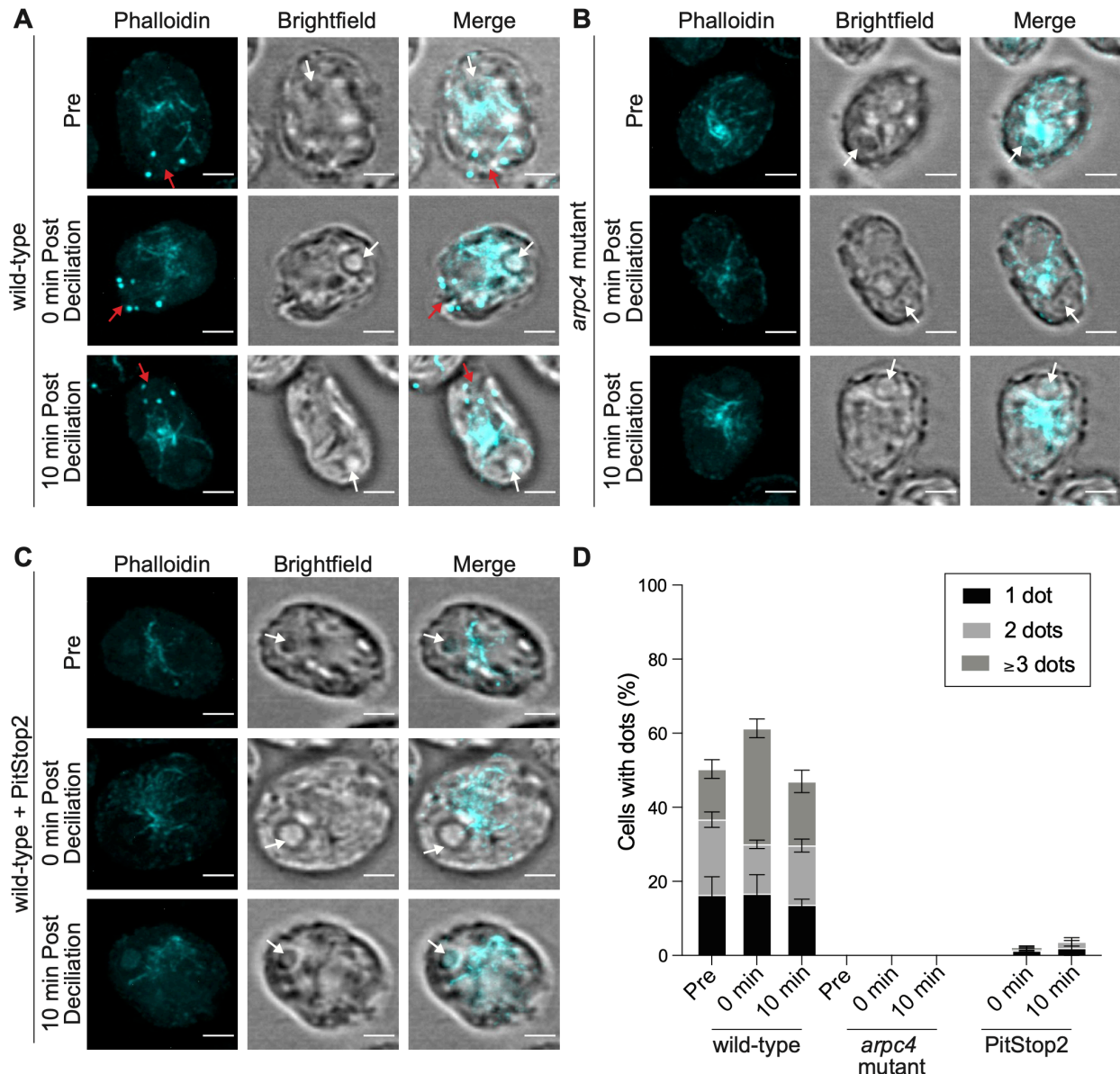
449  
 450

451 **Actin dots increase in an Arp2/3 complex and clathrin-dependent manner following**  
 452 **deciliation:**

453           Having established that the Arp2/3 complex is required for ciliary assembly, membrane  
454 dye internalization, and the endocytosis of a known ciliary protein, we wondered if these  
455 functions could be connected given that *arpc4* mutant cells have defects in maintaining cilia  
456 from non-Golgi sources (**Figure 3**). Therefore, we returned to the Arp2/3 complex-dependent  
457 actin dots seen in wild-type cells that are reminiscent of endocytic pits in yeast. Because ciliary  
458 membrane and proteins can come from the plasma membrane (Dentler, 2013), we suspected  
459 there would be an increase in these actin dots immediately following deciliation. We used  
460 phalloidin to visualize the actin cytoskeleton of wild-type cells before and immediately following  
461 deciliation, as well as 10 minutes later (**Figure 7A**). We saw an increase in both the percentage  
462 of cells with dots and the number of dots per cell immediately following deciliation that then  
463 returned to normal by 10 minutes (**Figure 7A and D**). This is consistent with the results shown  
464 in **Figure 1E-F** and confirms that the defect seen in ciliary assembly is due to an event  
465 occurring very early in ciliary assembly, even within the first few minutes after deciliation.

466           We wondered if this increase in dots would result in dots in the *arpc4* mutant cells which  
467 have almost not dots normally. We found that in the *arpc4* mutants dots were never observed,  
468 before or after deciliation (**Figure 7B and D**), suggesting these dots are dependent on the  
469 Arp2/3 complex. Next, we wanted to see if the dots really were due to clathrin-mediated  
470 endocytosis, so we treated cells with PitStop2 and looked for this same increase in dots. This  
471 treatment almost fully blocked the appearance of dots following deciliation and completely  
472 eliminated the presence of cells with 3 or more dots (**Figure 7C-D**), suggesting a clathrin-  
473 dependent mechanism, as well as an Arp2/3-dependent mechanism, is related to these dots.  
474



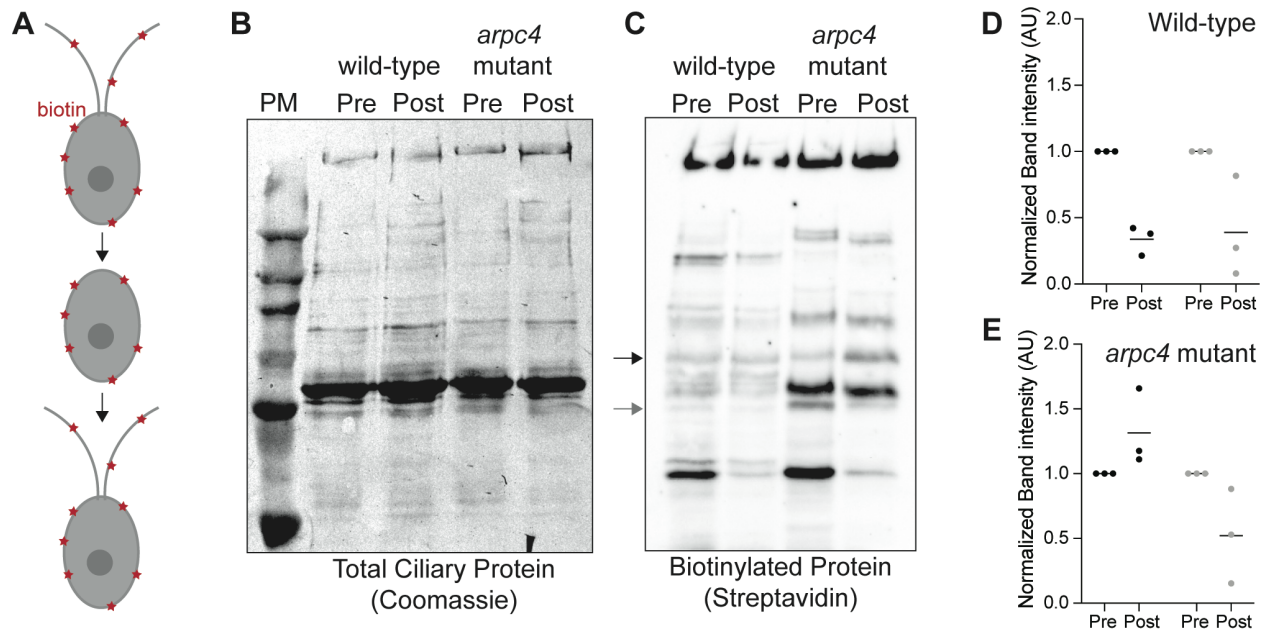


475  
 476 **Figure 7. Actin dots are clathrin and Arp2/3 complex-dependent.** A-C) Wild-type cells (A), *arpc4* mutant cells (B),  
 477 and wild-type cells treated with 30  $\mu$ M PitStop2 (C) stained with phalloidin to visualize the actin network before  
 478 deciliation, immediately following deciliation, and 10 minutes following deciliation. Brightfield images are to visualize  
 479 cell orientation. Images were taken as a z-stack using airyscan imaging and are shown as a maximum intensity  
 480 projection. Scale bar represents 2 $\mu$ m. Red arrows point to dots at the apex of the cell, and white arrows point to the  
 481 pyrenoid at the opposite end of the cell. D) The percentage of cells with 1 dot, 2 dot, or 3 dots in each condition.  
 482 Quantification based on sum slices of z-stacks taken using a spinning disk confocal. n=100 in 3 separate experiments.  
 483 For wild-type, the total number of cells with dots is significantly different for the 0 min time point (\*\*) and the number of  
 484 dotted cells with 3 or more dots is significantly different for the 0 time point (\*\*\*\*).  
 485  
 486

487 **Ciliary membrane proteins follow different paths from the plasma membrane to the cilia:**

488 Finally, to specifically determine if ciliary membrane and therefore membrane proteins  
 489 were coming from a pool in the plasma membrane we did an experiment first described in W.  
 490 Dentler 2013. Surface proteins were biotinylated, then cells were deciliated. After the cilia  
 491 regrew, they were isolated and probed for biotinylated protein (Figure 8A). Any biotinylated

492 protein present in the newly grown and isolated cilia must have come from a pool in the plasma  
 493 membrane. While some proteins returned in both wild-type and *arpc4* mutant cells, some  
 494 appeared to a lesser degree in *arpc4* mutant cells compared to wild-type cells (**Figure 8B-E,**  
 495 **black arrow and black bars**) and some returned to a higher degree in *arpc4* mutant cells  
 496 (**Figure 8B-E, grey arrow and grey bars**). Other biotinylated proteins found in wild-type cilia  
 497 were not found in the *arpc4* mutant cilia before or after deciliation, so there is a mechanism for  
 498 delivery of proteins to the cilia from the plasma membrane that Arp2/3 is absolutely essential for  
 499 (**Figure 8B-C**). This suggests there are multiple paths to the ciliary membrane, some of which  
 500 are Arp2/3 complex-independent and some that are Arp2/3 complex-dependent. This may  
 501 represent lateral diffusion and endocytosis respectively.  
 502  
 503  
 504  
 505



506  
 507 **Figure 8. Ciliary membrane proteins have multiple paths from the plasma membrane.** **A)** Cells were biotinylated,  
 508 deciliated, and then allowed to regrow before cilia were isolated and probed for biotinylated protein. **B)** Total protein in  
 509 wild-type and *arpc4* mutant ciliary isolate investigated by western blot and Coomassie. **C)** Wild-type and *arpc4* mutant  
 510 cells ciliary isolate was investigated by western blot and probed using streptavidin. Black arrow shows ciliary protein  
 511 present to a higher degree in wild-type cells than the *arpc4* mutant cells. Grey arrows show ciliary protein that is present  
 512 to a higher degree in *arpc4* mutant cells than in wild-type cells. **D)** Bands represented by black and grey arrows are  
 513 quantified for the wild-type cells. Data acquired from 3 separate experiments. **E)** Bands represented by black and grey  
 514 arrows are quantified for the *arpc4* mutant cells. Data represented as the mean from 3 separate experiments. Error  
 515 bars represent standard deviation.  
 516  
 517

## 518 DISCUSSION

519 In this study, we investigate the Arp2/3 complex of *Chlamydomonas reinhardtii* that  
 520 functions to maintain and assemble cilia. This complex potentially lacks the ARPC5 subunit,  
 521 although it is possible that a highly divergent ARPC5 exists. In yeast, deletion of any of the  
 522 genes encoding Arp2/3 complex members causes severe defects and even lethality, but these  
 523 defects differ in severity depending on the complex members deleted, suggesting that complex  
 524 members have varying degrees of importance in Arp2/3 complex function (Winter, Choe, and Li  
 525 1999). The role of ARPC5 in actin nucleation is being investigated, but some groups have found  
 526 it unnecessary for overall function of the complex (Gournier et al. 2001; von Loeffelholz et al.  
 527 2020). Furthermore, our data show that knocking out function of the ARPC5-less



528 *Chlamydomonas* Arp2/3 complex genetically or chemically results in phenotypes in ciliary  
529 assembly and maintenance, suggesting that the wild-type complex is active. Because the  
530 Arp2/3 complex has known functions in membrane dynamics, this led us to pursue models of  
531 Arp2/3 complex-dependent membrane trafficking to cilia.

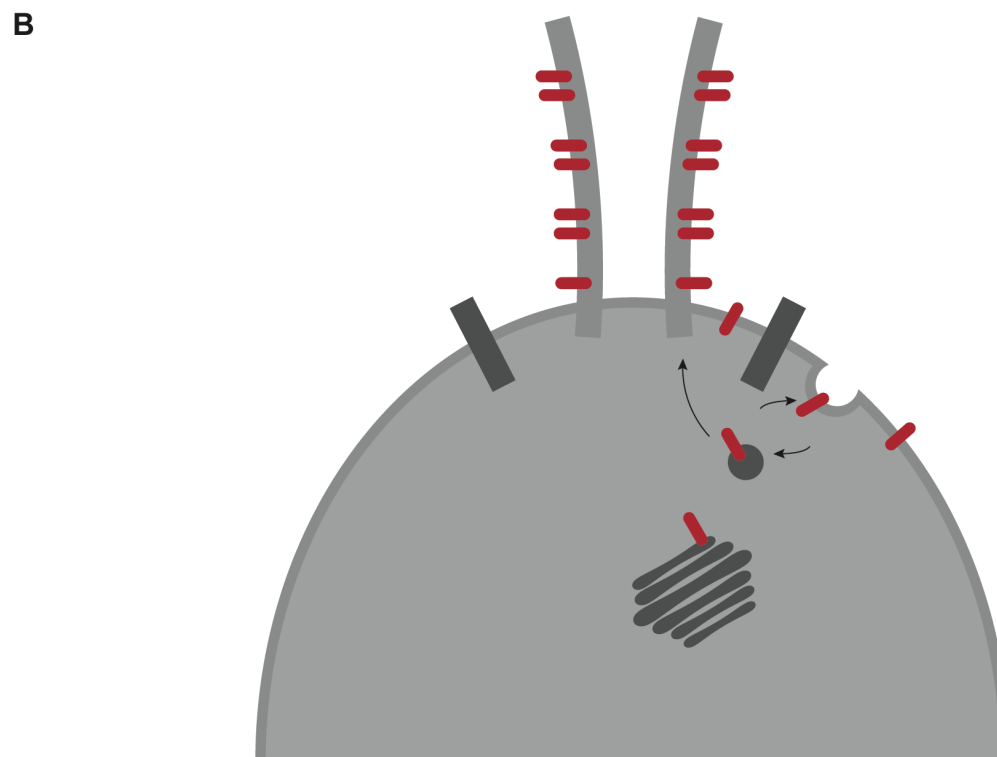
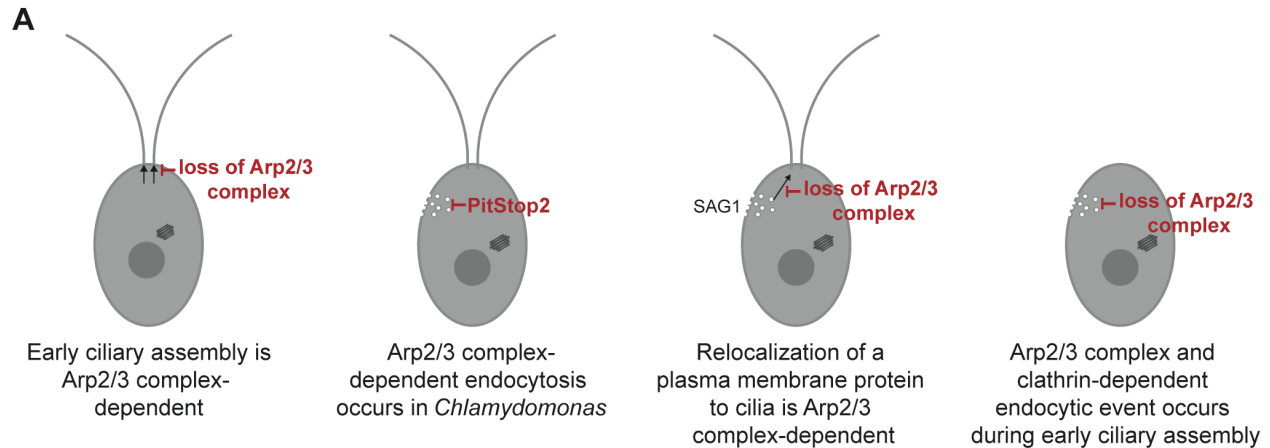
532 Previously, three models for the trafficking of membrane proteins to cilia have been  
533 proposed regarding where ciliary vesicles fuse relative to a diffusion barrier composed of  
534 septins (Hu Qicong et al. 2010), which delineates ciliary membrane and cell body plasma  
535 membrane (Nachury, Seeley, and Jin 2010). The first is that Golgi vesicles containing ciliary  
536 proteins fuse with the ciliary membrane inside the cilium itself. Proteins, both membrane and  
537 soluble, have been found to be transferred from the Golgi to the cilia on or in cytoplasmic  
538 vesicles (Wood and Rosenbaum 2014). Second, Golgi vesicles containing ciliary proteins fuse  
539 outside but near the cilium still within the diffusion barrier (Papermaster, Schneider, and  
540 Besharse 1985; Nachury et al. 2007; Zuo, Guo, and Lipschutz 2009). In *Chlamydomonas*, this  
541 was first described for mastigoneme proteins, which were found to be transferred from the Golgi  
542 and then exocytosed for use on the exterior of the cell (Bouck 1971). In the third model, Golgi  
543 vesicles containing proteins fuse with the plasma membrane outside the diffusion barrier where  
544 they somehow move in the plane of the plasma membrane across this barrier, perhaps through  
545 lateral diffusion that requires remodeling or passing through the diffusion barrier. Evidence for  
546 this path was shown using Hedgehog signaling protein Smoothed, which was found to  
547 relocalize in a dynamin-independent manner from the plasma membrane to the cilia  
548 immediately after stimulation in pulse labeling studies (Milenkovic, Scott, and Rohatgi 2009).

549 Our data support a fourth model, likely occurring in concert with other models, in which  
550 membrane proteins are recruited to the cilium from a reservoir in the cell body plasma  
551 membrane. We find that immediately following deciliation the Arp2/3 complex is required for  
552 ciliary assembly, clathrin-mediated endocytosis, and redistribution of ciliary proteins from the  
553 plasma membrane (**Figure 9A**). We hypothesize that ciliary membrane proteins and membrane  
554 targeted to the plasma membrane of the cell outside the diffusion barrier can be endocytosed  
555 and trafficked to cilia, either within or outside of the diffusion barrier in an actin and Arp2/3  
556 complex-dependent manner.

557 Although our data does not eliminate the possibility of Arp2/3 complex function in supply  
558 of ciliary membrane and protein stored in other endosomal compartments, ciliary localization of  
559 proteins initially labeled on the cell surface with biotin (**Figure 8**) suggests that some ciliary  
560 membrane proteins incorporated during assembly are coming directly from the plasma  
561 membrane itself. An endocytic mechanism of trafficking in intracellular ciliogenesis has been  
562 investigated previously in mammalian RPE1 cells. The ciliary pocket found at the base of  
563 primary and motile cilia formed intracellularly has been found to be an endocytically active  
564 region (Molla-Herman et al. 2010) but clathrin-mediated endocytosis was not required for  
565 ciliogenesis in those cells. The Bardet Biedl Syndrome complex (BBsome), which is involved in  
566 regulation of ciliary membrane protein composition, has been shown to interact with clathrin  
567 directly at the ciliary pocket to facilitate membrane sorting in trypanosomes (Langousis et al.  
568 2016). Further, some BBsome complex members resemble coat proteins such as clathrin (Jin et  
569 al. 2010) suggesting a direct role for the this cilium regulatory complex in membrane budding  
570 functions. It has also been found that disruption of recycling endosomes reduces the localization  
571 of polycystin-2 to cilia, suggesting a role for recycling endosomes in the localization of proteins  
572 to the cilia (Monis, Faundez, and Pazour 2017). Even in *Chlamydomonas*, clathrin heavy chain  
573 has been found to localize at the base of cilia (Kaplan et al. 2012). While the mechanism was  
574 unknown, it has been shown that plasma membrane surface-exposed proteins are relocalized to  
575 cilia during ciliary regeneration (W. Dentler 2013), a result we were able to recapitulate and  
576 demonstrate depends, in part, upon the Arp2/3 complex.

577 Altogether, this leads us to hypothesize that the role of the Arp2/3 complex in ciliary  
578 assembly is through endocytic recruitment from a ciliary protein reservoir in the plasma

579 membrane before newly synthesized protein and Golgi-derived membrane are capable of  
580 supplying additional materials (**Figure 9B**). While this model provides a possible route that  
581 some ciliary proteins and membranes take to the cilia, we believe this is one of several paths  
582 that can be taken to the cilia. Trafficking to cilia is likely cargo- and time-dependent, and which  
583 path proteins take may tell us the order and speed in which they populate the cilium for  
584 subsequent function.  
585



586  
587 **Figure 9. The Arp2/3 complex is required for membrane and protein delivery via a Golgi-independent,**  
588 **endocytosis-like process. A) Arp2/3-mediated actin networks are required for ciliary assembly in *Chlamydomonas***  
589 **particularly during the initial stages. These actin networks are also required for clathrin-mediated endocytosis, and for**  
590 **the endocytosis-like relocalization of a ciliary protein from the plasma membrane to the cilia. Finally, a large endocytic**  
591 **event occurs immediately following deciliation that is Arp2/3 complex-mediated and dependent on clathrin-mediated**  
592 **endocytosis. B) Proposed model of membrane protein and membrane transport from the plasma membrane to the cilia**  
593 **through endocytosis.**

594  
595  
596  
597  
598  
599  
600

## 601 METHODS

### 602 *Strains:*

603 The wild-type *Chlamydomonas* strain (CC-5325) and the *arpc4* mutant (LMJ.RY0402.232713)  
604 from the *Chlamydomonas* resource center. The *arpc4*:ARPC4-V5 strain was made by cloning  
605 the gene into pChlamy4 (*Chlamydomonas* resource center). Colonies were screened for the  
606 absence (in the case of the mutant) or presence (in the case of the rescue) by PCR using the  
607 primers AAAAGAATTCATGGCGCTCTCACTCAGGCCATA and  
608 AAAATCTAGACAGAAGGCAAGGGAGCGCAGGAA. The *nap1* mutant was a gift from Fred  
609 Cross, Masayuki Onishi, and John Pringle. The SAG1-HA strain was a gift from William Snell.  
610 Cells were grown and maintained on 1.5% Tris-Acetate Phosphate Agar (TAP) plates  
611 (*Chlamydomonas* resource center) under constant blue (450-475 nm) and red light (625-660  
612 nm). For experiments, cells were grown in liquid TAP media (*Chlamydomonas* resource center)  
613 overnight under constant red and blue light with agitation from a rotator. To induce gametes for  
614 mating for the SAG1-HA experiments, cells were grown in liquid M-N media (*Chlamydomonas*  
615 resource center) overnight with constant red and blue light and agitation.

616

### 617 *Ciliary studies:*

618 For steady state experiments, cells were treated with specified drugs [either 100 $\mu$ M CK-666,  
619 250 $\mu$ M CK-666 (Sigma, Burlington, MA), 250 $\mu$ M CK-689 (Sigma, Burlington, MA), 10 $\mu$ M LatB  
620 (Sigma, Burlington, MA), 10 $\mu$ M CHX (Sigma, Burlington, MA), or 36 $\mu$ M BFA (Sigma, Burlington,  
621 MA)] and incubated with agitation for the allotted times. Following any incubation (as well as a  
622 pre sample), cells were diluted in an equal volume of 2% glutaraldehyde and incubated at 4 $^{\circ}$   
623 Celsius until they sediment (within 24hrs). Following sedimentation, cells were imaged using a  
624 Zeiss DIC scope with a 40X objective. Cilia were then measured using the segmented line  
625 function in ImageJ. One cilia per cell was measured and 30 cilia total were measured.

626

627 For regeneration experiments, a pre sample was taken by adding cells to an equal volume of  
628 2% glutaraldehyde. Then cells were deciliated with 115 $\mu$ L of 0.5N acetic acid for 45 seconds.  
629 After this short incubation, the pH was returned to normal by adding 120 $\mu$ L of 0.5N KOH. A 0-  
630 minute sample was again taken by adding cells to an equal volume of 2% glutaraldehyde. Then  
631 cells were incubated with agitation and allowed to regrow cilia for the allotted time period with  
632 samples taken at the indicated time points by adding cells to an equal volume of 2%  
633 glutaraldehyde. Cells in glutaraldehyde were allowed to incubate at 4 $^{\circ}$  Celsius until  
634 sedimentation (within 24hrs). Then, cells were imaged using the same Zeiss DIC scope with a  
635 40X objective. Cilia were then measured using the segmented line function in ImageJ. One cilia  
636 per cell was measured and 30 cilia total were measured.

637

### 638 *Click-iT OPP Protein Synthesis Assay:*

639 Cells were grown overnight in TAP. The following day cells were deciliated as described above  
640 and allowed to regrow either with or without cycloheximide (10 $\mu$ M) to block protein synthesis. 1  
641 hour following deciliation, cells were mounted onto poly-lysine coverslips. Cells on coverslips  
642 were incubated with Click-iT OPP reagent containing the O-propargyl-puromycin (OPP) which is  
643 incorporated into nascent polypeptides for 30 minutes. OPP was removed and cells were

644 washed once in PBS. Cells were then fixed with 4% PFA in 1X HEPES for 15 minutes, then  
645 permeabilized with 0.5% Triton-X 100 in PBS for 15 minutes. Cells were washed twice with  
646 PBS. Detection was performed by incubating coverslips with 1X Click-iT OPP Reaction Cocktail  
647 that includes 1X Click-iT OPP Reaction Buffer, 1X Copper Protectant, 1X Alexafluor picolyl  
648 azide, and 1X Click-iT Reaction Buffer Additive for 30 minutes protected from light. This was  
649 removed and Reaction Rinse Buffer was added for 5 minutes. This was removed and coverslips  
650 were washed twice with PBS, allowed to dry fully, and mounted with Fluormount-G.

651  
652 Cells were then imaged on a Nikon Spinning Disk Confocal. Z-stacks were obtained then  
653 combined into sum slices for quantification of maximum intensity projections for viewing. In the  
654 summed images, the integrated density and area of individual cells was obtained, as well as the  
655 background fluorescence. These were then used to calculate CTCF, which was then normalized  
656 to the “Pre” sample for each cell.

657  
658 *Phalloidin staining and quantification:*

659 Procedure adapted from (Craig et al. 2019). Cells were mounted onto poly-lysine coverslips and  
660 fixed with fresh 4% paraformaldehyde in 1X HEPES. Coverslips with cells were then  
661 permeabilized with acetone and allowed to dry. Cells were rehydrated with PBS, stained with  
662 atto-phalloidin-488 (Sigma, Burlington, MA), and finally washed with PBS and allowed to dry  
663 before mounting with Fluoromount-G (Craig et al. 2019). Cells were imaged using the Nikon  
664 Spinning Disk Confocal. Z-stacks were obtained, and in ImageJ, maximum intensity projections  
665 were created for viewing.

666  
667 *Electron microscopy:*

668 Cells (1mL of each strain) were deciliated via pH shock by adding 115 $\mu$ L of 0.5N acetic acid for  
669 45 seconds followed by 120 $\mu$ L of 0.5N KOH to bring cells back to neutral pH. Cells were  
670 allowed to regrow cilia for 30 minutes. A pre sample and a 30-minute post-deciliation sample  
671 were fixed in an equal volume of 2% glutaraldehyde for 20 minutes at room temperature.  
672 Samples were then pelleted using gentle centrifugation for 10 minutes. The supernatant was  
673 removed, and cells were resuspended in 1% glutaraldehyde, 20mM sodium cacodylate. Cells  
674 were incubated for 1 hour at room temperature and then overnight at 4° Celsius. This protocol  
675 was first reported in (W. L. Dentler and Adams 1992).

676  
677 *SAG1-HA Immunofluorescence:*

678 Procedure adapted from (Belzile et al. 2013). SAG1-HA cells were grown overnight in M-N  
679 media to induce gametes. These cells were then treated with either 10 $\mu$ M LatB for 1 hour or  
680 250 $\mu$ M CK-666 for 2 hours. Following treatment, mating was induced by adding db-cAMP  
681 (ChemCruz, Santa Cruz, CA) to a final concentration of 13.5mM and incubating for 30 minutes.  
682 Cells were adhered to coverslips and fixed with methanol. Cells were then dried and rehydrated  
683 with PBS and incubated with 100% block (5% BSA, 1% fish gelatin) for 30 minutes. The 100%  
684 block was replaced with new 100% block containing 10% normal goat serum for another 30-  
685 minute incubation. The primary antibody (rat anti-HA, Sigma, Burlington, MA) was diluted  
686 1:1000 in 20% block in PBS. Coverslips were incubated at 4° Celsius in a humidified chamber  
687 overnight. The primary antibody was removed and washed away with 3 10-minute PBS washes.  
688 The secondary (anti-rat IgG-Alexafluor 488, Invitrogen, Carlsbad, CA) was added and coverslips  
689 were incubated at room temperature for 1 hour. This was followed by 3 more 10-minute PBS  
690 washes and finally mounting with Fluoromount-G. Cells were imaged using a Nikon widefield  
691 microscope. Z-stacks were obtained, and maximum intensity projections were created for  
692 visualization and sum slices were created for quantification using ImageJ.

693

694 Images were quantified by using line scans from the apex of the cells to the basal region of the  
695 cells farthest away from the apex. Line scans were then normalized, and background subtracted  
696 before being combined into single graphs. Using the line scans, the intensity of signal at the  
697 basal region of the cells was subtracted from the signal at the apical region. Finally, cells with a  
698 difference over 30 were considered to be apically enriched and this was quantified as  
699 percentage of cells with apical staining.

700

701 *SAG1-HA western blot:*

702 Procedure adapted from (Belzile et al. 2013). SAG1-HA cells were grown overnight in M-N  
703 media to induce gametes. These cells were then treated with either 10 $\mu$ M LatB for 1 hour or  
704 250 $\mu$ M CK-666 for 2 hours. Following treatment, mating induction was done by adding db-cAMP  
705 to a final concentration of 13.5mM and incubating for 10 minutes. Cells were then treated with  
706 0.01% trypsin for 5 minutes, pelleted (at 500xg for 2 minutes), resuspended in lysis buffer (5%  
707 glycerol, 1% NP-40, 1mM DTT, 1X protease inhibitors), and then lysed with bead beating. Cell  
708 debris was spun down at 14000xg for 15 minutes. An equal amount of protein was loaded to a  
709 10% SDS-PAGE gel. The resulting gel was transferred to membrane which was then blocked  
710 with 5% milk in PBST. The primary antibody (rabbit anti-HA, Cell Signaling, Danvers, MA)  
711 diluted to 1:1000 in 1% BSA, 1% milk was added and incubated overnight at 4 $^{\circ}$  Celsius. Primary  
712 antibody washed off with 3 10-minute PBST washes. Secondary antibody (anti rabbit IgG,  
713 Invitrogen, Carlsbad, CA) was diluted to 1:5000 in 1% milk. 1% BSA was added, and the blot  
714 was incubated for 1 hour. Membrane was probed with West Pico Chemiluminescent Pico  
715 Substrate (Invitrogen, Carlsbad, CA). The same membrane was stripped of antibody and total  
716 protein was determined with amido black staining. Band intensity was measured in ImageJ and  
717 normalized to total protein

718

719 *Membrane stain:*

720 FM 4-64FX membrane stain (Thermo, Waltham, MA) was diluted to a stock concentration of  
721 200 $\mu$ g/mL. Cells were adhered to poly-lysine coverslips. After a 5-minute incubation, cells were  
722 tilted off and 5 $\mu$ g/mL of ice-cold stain in Hank's Buffered Salt Solution (HBSS) without  
723 magnesium or calcium was added for 1 minute. The stain was tilted off and cells were fixed with  
724 ice cold 4% paraformaldehyde in HBSS without magnesium or calcium for 15 minutes.  
725 Coverslips were then rinsed 3 times for 10 minutes each in ice cold HBSS without magnesium  
726 or calcium. Finally, cells were mounted with Fluoromount-G and imaged using the Nikon  
727 Spinning Disk Confocal. Z-stacks were taken and combined into sum projections using ImageJ.  
728 The background corrected total cell fluorescence was then calculated by taking the integrated  
729 density and subtracting the sum of the area and the mean background intensity.

730

731 *Clathrin light chain immunofluorescence:*

732 Cells were grown overnight in TAP media. Cells were deciliated using low pH shock. Cells are  
733 then adhered to coverslips and fixed with 4% PFA in 1X HEPES. Cells were then dried and  
734 rehydrated with PBS and incubated with 100% block (5% BSA, 1% fish gelatin) for 1 hour. The  
735 primary antibody (goat anti-clathrin light chain, Abcam, Cambridge, UK or rabbit anti-acetylated  
736 tubulin, Cell Signaling, Danvers, MA) was diluted 1:1000 in 20% block in PBS. Coverslips were  
737 incubated at 4 $^{\circ}$  Celsius in a humidified chamber overnight. The primary antibody was removed  
738 and washed away with 3 10-minute PBS washes. The secondary (donkey anti-goat IgG-  
739 Alexafluor 488, Invitrogen, Carlsbad, CA or goat anti-rabbit IgG-Alexafluor 568, Invitrogen,  
740 Carlsbad, CA) was added and coverslips were incubated at room temperature for 1 hour. For  
741 cells stained with DAPI, DAPI (Biotium, Fremont, CA) was added for the last 10 minutes of  
742 secondary antibody incubation. This was followed by 3 more 10-minute PBS washes and finally  
743 mounting with Fluoromount-G. Cells were imaged using a Nikon widefield microscope. Z-stacks



744 were obtained, and maximum intensity projections were created for visualization and sum slices  
745 were created for quantification using ImageJ.

746

747 *Biotin ciliary isolation:*

748 Procedure adapted from (W. Dentler 2013). 100mL of cells were grown in TAP for each  
749 condition until they reached an OD<sub>730</sub> of 1.6 or above. Cells were then spun down and  
750 resuspended in M1 media and allowed to grow overnight. The next day cells were spun down at  
751 1800rpm for 3 minutes and resuspended in HM Media (10mM HEPES, 5mM MgSO<sub>4</sub>, pH 7.2).  
752 Solid biotin (Thermo, Waltham, MA) was added to 20µg/mL for each strain and incubated for 5  
753 minutes with agitation. Cells were diluted with 10 volumes of fresh M1 media before being spun  
754 down at 1800rpm for 3 minutes. After all cells were pelleted, they were washed with fresh M1  
755 media three times. A pre sample was set aside (100mL) and the remainder of the cells were  
756 resuspended in 4.5 pH M1 media for 45 seconds before being spun down again at 1800rpm for  
757 3 minutes. Cells were then resuspended in pH 7.0 media and allowed to regrow their cilia for 4  
758 hours. A sample was taken pre-biotinylation to use as a control for non-specific streptavidin  
759 binding.

760

761 Meanwhile, the cilia were isolated from the pre sample. The samples were centrifuged for 3  
762 minutes at 1800rpm. Supernatant was drained and each pellet was resuspended in 2 mL of  
763 10mM HEPES (pH 7.4). This was repeated 2 times. Then each pellet was resuspended in 1 mL  
764 of fresh ice-cold 4% HMDS (10mM HEPES pH 7.4, 5mM MgSO<sub>4</sub>, 1mM DTT, 4% w/v sucrose).  
765 Cells were deciliated by incubating with 25mM dibucaine for 2 minutes. Then ice cold HMDS  
766 with 0.5mM EGTA was added (1mL per 1.5mL of cells). This was then centrifuged for 3 minutes  
767 at 1800rpm. Supernatant was collected for each sample. Then HMDS with 25% sucrose was  
768 layered beneath the supernatant (2 mL of 25% HMDS for 1mL of supernatant) to create an  
769 interface. This was centrifuged at 4° Celsius for 10 min at 2400rpm with no brake to avoid  
770 disrupting interface where cilia should now be located. Cilia were removed, pelleted at 21130xg  
771 for 30 minutes, then resuspended in lysis buffer (5% glycerol, 1% NP-40, 1mM DTT, 1X  
772 protease inhibitors). This was repeated with the post samples 4 hours following deciliation. An  
773 equal amount of protein was loaded to a 10% SDS-PAGE gel. The resulting gel was transferred  
774 to PVDF membrane. The membrane was washed 2x with PBSAT (PBST + 0.1% BSA), then  
775 incubated with HRP-conjugated streptavidin (Thermo, Waltham, MA) for 1 hour. The membrane  
776 was then washed 3 times with PBSAT (10 minutes each) and 3 times with PBST (15 minutes  
777 each). Membrane was probed with West Pico Chemiluminescent Pico Substrate (Invitrogen,  
778 Carlsbad, CA). The same membrane was stripped of antibody and incubated with Coomassie  
779 Brilliant Blue to observe total protein.

780

781 *Homology modeling and sequence studies:*

782 Arp2/3 homology model was created using the Modeller plugin in UCSF Chimera. The template  
783 used was 1U2Z (Nolen, Littlefield, and Pollard 2004; Sali and Blundell 1993; Pettersen et al.  
784 2004). Percent identity and similarity is calculated in relation to the human Arp2/3 complex  
785 members using a MUSCLE alignment in Geneious. The homology model was visualized and  
786 conservation was mapped on the protein surface using Chimera (Pettersen et al. 2004).

787

788 *Statistical analysis:*

789 Statistical analyses were done if GraphPad Prism Version 9. Superplots were created using the  
790 method in (Lord et al. 2020). For any experiments comparing 2 groups (**Figure 3D, 5C, and 5E**)  
791 an unpaired student's t-test was used to determine P value. For experiments comparing multiple  
792 samples at a single time point (**Figure 1A, 1B, and 2B**), an ANOVA was used. Finally, for any  
793 graphs covering several time points (**Figure 1C, 1D, 2C, 3B, and 6E**), multiple comparisons

794 were performed (Tukey's and Sidak's). For any percentages shown (**Figure 7D**), Chi-squared  
795 analysis was performed. For all experiments \*\*\*\* P<0.0001, \*\*\* P<0.001, \*\* P<0.01, \* P<0.1.

796  
797

#### 798 **ACKNOWLEDGEMENTS:**

799 Our most sincere gratitude to William Dentler for providing his expertise especially in  
800 looking at the electron microscopy images and for his helpful advice, William Snell for  
801 generously providing the SAG1-HA strain, Masayuki Onishi for generously providing the *nap1*  
802 mutant strain, Henry Higgs for his feedback on version 1 of the manuscript, Ann Lavanway for  
803 assistance with microscopy, and the Avasthi lab for all their help throughout the project. We  
804 would also like to thank David Sept and Courtney M Schroeder for the help with the original  
805 version of this paper and for providing helpful comments throughout the process.

806 We also thank our funding sources including the Madison and Lila Self Graduate  
807 Fellowship at the University of Kansas Medical Center and the MIRA (R35GM128702). Finally,  
808 we thank the BioMT core at Dartmouth College (NIH/NIGMS COBRE award P20-GM113132),  
809 the Genomics and Molecular Biology Shared Resources Core (NCI Cancer Center Support  
810 Grant 5P30CA023108-37), and the KIDDRC NIH U54 HD 090216 at the University of Kansas  
811 Medical Center, Kansas City, KS 66160.

812  
813

#### 814 **REFERENCES:**

- 815 Adams, A E, and J R Pringle. 1984. "Relationship of Actin and Tubulin Distribution to Bud  
816 Growth in Wild-Type and Morphogenetic-Mutant *Saccharomyces Cerevisiae*." *Journal of*  
817 *Cell Biology* 98 (3): 934–45. <https://doi.org/10.1083/jcb.98.3.934>.
- 818 Aghamohammadzadeh, Soheil, and Kathryn R. Ayscough. 2009. "Differential Requirements for  
819 Actin during Yeast and Mammalian Endocytosis." *Nature Cell Biology* 11 (8): 1039–42.  
820 <https://doi.org/10.1038/ncb1918>.
- 821 Avasthi, Prachee, Masayuki Onishi, Joel Karpiak, Ryosuke Yamamoto, Luke Mackinder, Martin C  
822 Jonikas, Winfield S Sale, Brian Shoichet, John R Pringle, and Wallace F Marshall. 2014.  
823 "Actin Is Required for IFT Regulation in *Chlamydomonas Reinhardtii*." *Current Biology* 24  
824 (17): 2025–32. <https://doi.org/10.1016/j.cub.2014.07.038>.
- 825 Ayscough, K. R., J. Stryker, N. Pokala, M. Sanders, P. Crews, and D. G. Drubin. 1997. "High Rates  
826 of Actin Filament Turnover in Budding Yeast and Roles for Actin in Establishment and  
827 Maintenance of Cell Polarity Revealed Using the Actin Inhibitor Latrunculin-A." *The*  
828 *Journal of Cell Biology* 137 (2): 399–416. <https://doi.org/10.1083/jcb.137.2.399>.
- 829 Basu, Roshni, Emilia Laura Munteanu, and Fred Chang. 2014. "Role of Turgor Pressure in  
830 Endocytosis in Fission Yeast." *Molecular Biology of the Cell* 25 (5): 679–87.  
831 <https://doi.org/10.1091/mbc.E13-10-0618>.
- 832 Belzile, Olivier, Carmen I Hernandez-Lara, Qian Wang, and William J Snell. 2013. "Regulated  
833 Membrane Protein Entry into Flagella Is Facilitated by Cytoplasmic Microtubules and  
834 Does Not Require IFT." *Current Biology : CB* 23 (15): 1460–65.  
835 <https://doi.org/10.1016/j.cub.2013.06.025>.
- 836 Bouck, G. Benjamin. 1971. "THE STRUCTURE, ORIGIN, ISOLATION, AND COMPOSITION OF THE  
837 TUBULAR MASTIGONEMES OF THE OCHROMONAS FLAGELLUM." *Journal of Cell Biology*  
838 50 (2): 362–84. <https://doi.org/10.1083/jcb.50.2.362>.
- 839 Campellone, K., and M. Welch. 2010. "A Nucleator Arms Race: Cellular Control of Actin  
840 Assembly." *Nature Reviews Molecular Cell Biology* 11: 237–51.



- 841 Carlsson, Anders E., and Philip V. Bayly. 2014. "Force Generation by Endocytic Actin Patches in  
842 Budding Yeast." *Biophysical Journal* 106 (8): 1596–1606.  
843 <https://doi.org/10.1016/j.bpj.2014.02.035>.
- 844 Cheng, Xi, Gai Liu, Wenting Ke, Lijuan Zhao, Bo Lv, Xiaocui Ma, Nannan Xu, et al. 2017. "Building  
845 a Multipurpose Insertional Mutant Library for Forward and Reverse Genetics in  
846 Chlamydomonas." *Plant Methods* 13 (1): 36. [https://doi.org/10.1186/s13007-017-0183-](https://doi.org/10.1186/s13007-017-0183-5)  
847 5.
- 848 Cochilla, Amanda J., Joseph K. Angleson, and William J. Betz. 1999. "MONITORING SECRETORY  
849 MEMBRANE WITH FM1-43 FLUORESCENCE." *Annual Review of Neuroscience* 22 (1): 1–  
850 10. <https://doi.org/10.1146/annurev.neuro.22.1.1>.
- 851 Craig, Evan W., David M. Mueller, Brae M. Bigge, Miroslava Schaffer, Benjamin D. Engel, and  
852 Prachee Avasthi. 2019. "The Elusive Actin Cytoskeleton of a Green Alga Expressing Both  
853 Conventional and Divergent Actins." *Molecular Biology of the Cell*, mbc.E19-03-0141.  
854 <https://doi.org/10.1091/mbc.E19-03-0141>.
- 855 Dentler, W L, and C Adams. 1992. "Flagellar Microtubule Dynamics in Chlamydomonas:  
856 Cytochalasin D Induces Periods of Microtubule Shortening and Elongation; and  
857 Colchicine Induces Disassembly of the Distal, but Not Proximal, Half of the Flagellum."  
858 *The Journal of Cell Biology* 117 (6): 1289–98. <https://doi.org/10.1083/jcb.117.6.1289>.
- 859 Dentler, William. 2013. "A Role for the Membrane in Regulating Chlamydomonas Flagellar  
860 Length." *PLOS ONE* 8 (1): e53366. <https://doi.org/10.1371/journal.pone.0053366>.
- 861 Diener, Dennis R, Pietro Lupetti, and Joel L Rosenbaum. 2015. "Proteomic Analysis of Isolated  
862 Ciliary Transition Zones Reveals the Presence of ESCRT Proteins." *Current Biology : CB* 25  
863 (3): 379–84. <https://doi.org/10.1016/j.cub.2014.11.066>.
- 864 Farina, Francesca, Jérémie Gaillard, Christophe Guérin, Yohann Couté, James Sillibourne,  
865 Laurent Blanchoin, and Manuel Théry. 2016. "The Centrosome Is an Actin-Organizing  
866 Centre." *Nature Cell Biology* 18 (1): 65–75. <https://doi.org/10.1038/ncb3285>.
- 867 Gachet, Yannick, and Jeremy S. Hyams. 2005. "Endocytosis in Fission Yeast Is Spatially  
868 Associated with the Actin Cytoskeleton during Polarised Cell Growth and Cytokinesis."  
869 *Journal of Cell Science* 118 (Pt 18): 4231–42. <https://doi.org/10.1242/jcs.02530>.
- 870 Goode, Bruce L, Julian A Eskin, and Beverly Wendland. 2015. "Actin and Endocytosis in Budding  
871 Yeast." *Genetics* 199 (2): 315–58. <https://doi.org/10.1534/genetics.112.145540>.
- 872 Gournier, Helene, Erin D. Goley, Hanspeter Niederstrasser, Thong Trinh, and Matthew D.  
873 Welch. 2001. "Reconstitution of Human Arp2/3 Complex Reveals Critical Roles of  
874 Individual Subunits in Complex Structure and Activity." *Molecular Cell* 8 (5): 1041–52.  
875 [https://doi.org/10.1016/S1097-2765\(01\)00393-8](https://doi.org/10.1016/S1097-2765(01)00393-8).
- 876 Hetrick, Byron, Min Suk Han, Luke A Helgeson, and Brad J Nolen. 2013. "Small Molecules CK-666  
877 and CK-869 Inhibit Actin-Related Protein 2/3 Complex by Blocking an Activating  
878 Conformational Change." *Chemistry & Biology* 20 (5): 701–12.  
879 <https://doi.org/10.1016/j.chembiol.2013.03.019>.
- 880 Hirono, Masafumi, Satomi Uryu, Akio Ohara, Takako Kato-Minoura, and Ritsu Kamiya. 2003.  
881 "Expression of Conventional and Unconventional Actins in Chlamydomonas Reinhardtii  
882 upon Deflagellation and Sexual Adhesion." *Eukaryotic Cell* 2 (3): 486–93.  
883 <https://doi.org/10.1128/ec.2.3.486-493.2003>.

- 884 Hu Qicong, Milenkovic Ljiljana, Jin Hua, Scott Matthew P., Nachury Maxence V., Spiliotis Elias T.,  
885 and Nelson W. James. 2010. "A Septin Diffusion Barrier at the Base of the Primary Cilium  
886 Maintains Ciliary Membrane Protein Distribution." *Science* 329 (5990): 436–39.  
887 <https://doi.org/10.1126/science.1191054>.
- 888 Inoue, Daisuke, Dorian Obino, Judith Pineau, Francesca Farina, Jérémie Gaillard, Christophe  
889 Guerin, Laurent Blanchoin, Ana-Maria Lennon-Duménil, and Manuel Théry. 2019. "Actin  
890 Filaments Regulate Microtubule Growth at the Centrosome." *The EMBO Journal* 38 (11).  
891 <https://doi.org/10.15252/embj.201899630>.
- 892 Jack, Brittany, and Prachee Avasthi. 2018. "Erratum to: Chemical Screening for Flagella-  
893 Associated Phenotypes in *Chlamydomonas Reinhardtii*." *Methods in Molecular Biology*  
894 (*Clifton, N.J.*) 1795: E1. [https://doi.org/10.1007/978-1-4939-7874-8\\_19](https://doi.org/10.1007/978-1-4939-7874-8_19).
- 895 Jack, Brittany, David M. Mueller, Ann C. Fee, Ashley L. Tetlow, and Prachee Avasthi. 2019.  
896 "Partially Redundant Actin Genes in *Chlamydomonas* Control Transition Zone  
897 Organization and Flagellum-Directed Traffic." *Cell Reports* 27 (8): 2459-2467.e3.  
898 <https://doi.org/10.1016/j.celrep.2019.04.087>.
- 899 Jin, Hua, Susan Roehl White, Toshinobu Shida, Stefan Schulz, Mike Aguiar, Steven P. Gygi, J.  
900 Fernando Bazan, and Maxence V. Nachury. 2010. "The Conserved Bardet-Biedl  
901 Syndrome Proteins Assemble a Coat That Traffics Membrane Proteins to Cilia." *Cell* 141  
902 (7): 1208–19. <https://doi.org/10.1016/j.cell.2010.05.015>.
- 903 Kaplan, Oktay I., David B. Doroquez, Sebiha Cevik, Rachel V. Bowie, Lara Clarke, Anna A.W.M.  
904 Sanders, Katarzyna Kida, Joshua Z. Rappoport, Piali Sengupta, and Oliver E. Blacque.  
905 2012. "Endocytosis Genes Facilitate Protein and Membrane Transport in *C. Elegans*  
906 Sensory Cilia." *Current Biology* 22 (6): 451–60.  
907 <https://doi.org/10.1016/j.cub.2012.01.060>.
- 908 Kato-Minoura, T, S Uryu, M Hirono, and R Kamiya. 1998. "Highly Divergent Actin Expressed in a  
909 *Chlamydomonas* Mutant Lacking the Conventional Actin Gene." *Biochemical and*  
910 *Biophysical Research Communications* 251 (1): 71–76.  
911 <https://doi.org/10.1006/bbrc.1998.9373>.
- 912 Kiesel, Petra, Gonzalo Alvarez Viar, Nikolai Tsoy, Riccardo Maraspini, Peter Gorilak, Vladimir  
913 Varga, Alf Honigmann, and Gaia Pigino. 2020. "The Molecular Structure of Mammalian  
914 Primary Cilia Revealed by Cryo-Electron Tomography." *Nature Structural & Molecular*  
915 *Biology*, September. <https://doi.org/10.1038/s41594-020-0507-4>.
- 916 Kim, Joon, Ji Eun Lee, Susanne Heynen-Genel, Eigo Suyama, Keiichiro Ono, Kiyoung Lee, Trey  
917 Ideker, Pedro Aza-Blanc, and Joseph G. Gleeson. 2010. "Functional Genomic Screen for  
918 Modulators of Ciliogenesis and Cilium Length." *Nature* 464 (7291): 1048–51.  
919 <https://doi.org/10.1038/nature08895>.
- 920 Langousis, Gerasimos, Michelle M. Shimogawa, Edwin A. Saada, Ajay A. Vashisht, Roberto  
921 Spreafico, Andrew R. Nager, William D. Barshop, Maxence V. Nachury, James A.  
922 Wohlschlegel, and Kent L. Hill. 2016. "Loss of the BBSome Perturbs Endocytic Trafficking  
923 and Disrupts Virulence of *Trypanosoma Brucei*." *Proceedings of the National Academy*  
924 *of Sciences of the United States of America* 113 (3): 632–37.  
925 <https://doi.org/10.1073/pnas.1518079113>.
- 926 Lefebvre, P. A., S. A. Nordstrom, J. E. Moulder, and J. L. Rosenbaum. 1978. "Flagellar Elongation  
927 and Shortening in *Chlamydomonas*. IV. Effects of Flagellar Detachment, Regeneration,

- 928 and Resorption on the Induction of Flagellar Protein Synthesis." *The Journal of Cell*  
929 *Biology* 78 (1): 8–27. <https://doi.org/10.1083/jcb.78.1.8>.
- 930 Lefebvre, Paul A. 1995. "Flagellar Amputation and Regeneration in Chlamydomonas." In  
931 *Methods in Cell Biology*, 47:3–7. Elsevier.
- 932 Li, Xiaobo, Weronika Patena, Friedrich Fauser, Robert E. Jinkerson, Shai Saroussi, Moritz T.  
933 Meyer, Nina Ivanova, et al. 2019. "A Genome-Wide Algal Mutant Library and Functional  
934 Screen Identifies Genes Required for Eukaryotic Photosynthesis." *Nature Genetics* 51  
935 (4): 627–35. <https://doi.org/10.1038/s41588-019-0370-6>.
- 936 Loeffelholz, Ottilie von, Andrew Purkiss, Luyan Cao, Svend Kjaer, Naoko Kogata, Guillaume  
937 Romet-Lemonne, Michael Way, and Carolyn A. Moores. 2020. "Cryo-EM of Human  
938 Arp2/3 Complexes Provides Structural Insights into Actin Nucleation Modulation by  
939 ARPC5 Isoforms." *BioRxiv*, January, 2020.05.01.071704.  
940 <https://doi.org/10.1101/2020.05.01.071704>.
- 941 Lord, Samuel J., Katrina B. Velle, R. Dyche Mullins, and Lillian K. Fritz-Laylin. 2020. "SuperPlots:  
942 Communicating Reproducibility and Variability in Cell Biology." *The Journal of Cell*  
943 *Biology* 219 (6). <https://doi.org/10.1083/jcb.202001064>.
- 944 Macia, Eric, Marcelo Ehrlich, Ramiro Massol, Emmanuel Boucrot, Christian Brunner, and Tomas  
945 Kirchhausen. 2006. "Dynasore, a Cell-Permeable Inhibitor of Dynamin." *Developmental*  
946 *Cell* 10 (6): 839–50. <https://doi.org/10.1016/j.devcel.2006.04.002>.
- 947 Milenkovic, Ljiljana, Matthew P. Scott, and Rajat Rohatgi. 2009. "Lateral Transport of  
948 Smoothed from the Plasma Membrane to the Membrane of the Cilium." *The Journal*  
949 *of Cell Biology* 187 (3): 365–74. <https://doi.org/10.1083/jcb.200907126>.
- 950 Molla-Herman, Anahi, Rania Ghossoub, Thierry Blisnick, Alice Meunier, Catherine Serres, Flora  
951 Silbermann, Chris Emmerson, et al. 2010. "The Ciliary Pocket: An Endocytic Membrane  
952 Domain at the Base of Primary and Motile Cilia." *Journal of Cell Science* 123 (Pt 10):  
953 1785–95. <https://doi.org/10.1242/jcs.059519>.
- 954 Monis, William J., Victor Faundez, and Gregory J. Pazour. 2017. "BLOC-1 Is Required for  
955 Selective Membrane Protein Trafficking from Endosomes to Primary Cilia." *The Journal*  
956 *of Cell Biology* 216 (7): 2131–50. <https://doi.org/10.1083/jcb.201611138>.
- 957 Nachury, Maxence V., Alexander V. Loktev, Qihong Zhang, Christopher J. Westlake, Johan  
958 Peränen, Andreas Merdes, Diane C. Slusarski, et al. 2007. "A Core Complex of BBS  
959 Proteins Cooperates with the GTPase Rab8 to Promote Ciliary Membrane Biogenesis."  
960 *Cell* 129 (6): 1201–13. <https://doi.org/10.1016/j.cell.2007.03.053>.
- 961 Nachury, Maxence V., E. Scott Seeley, and Hua Jin. 2010. "Trafficking to the Ciliary Membrane:  
962 How to Get across the Periciliary Diffusion Barrier?" *Annual Review of Cell and*  
963 *Developmental Biology* 26: 59–87.  
964 <https://doi.org/10.1146/annurev.cellbio.042308.113337>.
- 965 Nolen, Brad J., Ryan S. Littlefield, and Thomas D. Pollard. 2004. "Crystal Structures of Actin-  
966 Related Protein 2/3 Complex with Bound ATP or ADP." *Proceedings of the National*  
967 *Academy of Sciences of the United States of America* 101 (44): 15627.  
968 <https://doi.org/10.1073/pnas.0407149101>.
- 969 Onishi, M., K. Pecani, T. th Jones, J. R. Pringle, and F. R. Cross. 2018. "F-Actin Homeostasis  
970 through Transcriptional Regulation and Proteasome-Mediated Proteolysis." *Proc Natl*  
971 *Acad Sci U S A* 115 (28): E6487–e6496. <https://doi.org/10.1073/pnas.1721935115>.

- 972 Onishi, M., J. R. Pringle, and F. R. Cross. 2016. "Evidence That an Unconventional Actin Can  
973 Provide Essential F-Actin Function and That a Surveillance System Monitors F-Actin  
974 Integrity in *Chlamydomonas*." *Genetics* 202 (3): 977–96.  
975 <https://doi.org/10.1534/genetics.115.184663>.
- 976 Onishi, Masayuki, James G. Umen, Frederick R. Cross, and John R. Pringle. 2019. "Cleavage-  
977 Furrow Formation without F-Actin in *Chlamydomonas*." *BioRxiv*, January,  
978 789016. <https://doi.org/10.1101/789016>.
- 979 Papermaster, D. S., B. G. Schneider, and J. C. Besharse. 1985. "Vesicular Transport of Newly  
980 Synthesized Opsin from the Golgi Apparatus toward the Rod Outer Segment.  
981 Ultrastructural Immunocytochemical and Autoradiographic Evidence in *Xenopus*  
982 Retinas." *Investigative Ophthalmology & Visual Science* 26 (10): 1386–1404.
- 983 Park, Tae Joo, Brian J. Mitchell, Philip B. Abitua, Chris Kintner, and John B. Wallingford. 2008.  
984 "Dishevelled Controls Apical Docking and Planar Polarization of Basal Bodies in Ciliated  
985 Epithelial Cells." *Nature Genetics* 40 (7): 871–79. <https://doi.org/10.1038/ng.104>.
- 986 Pasquale, S M, and U W Goodenough. 1987. "Cyclic AMP Functions as a Primary Sexual Signal in  
987 Gametes of *Chlamydomonas Reinhardtii*." *The Journal of Cell Biology* 105 (5): 2279–92.  
988 <https://doi.org/10.1083/jcb.105.5.2279>.
- 989 Pedersen, Lotte B., and Joel L. Rosenbaum. 2008. "Intraflagellar Transport (IFT) Role in Ciliary  
990 Assembly, Resorption and Signalling." *Current Topics in Developmental Biology* 85: 23–  
991 61. [https://doi.org/10.1016/S0070-2153\(08\)00802-8](https://doi.org/10.1016/S0070-2153(08)00802-8).
- 992 Pettersen, Eric F., Thomas D. Goddard, Conrad C. Huang, Gregory S. Couch, Daniel M.  
993 Greenblatt, Elaine C. Meng, and Thomas E. Ferrin. 2004. "UCSF Chimera--a Visualization  
994 System for Exploratory Research and Analysis." *Journal of Computational Chemistry* 25  
995 (13): 1605–12. <https://doi.org/10.1002/jcc.20084>.
- 996 Ranjan, Peeyush, Mayanka Awasthi, and William J. Snell. 2019. "Transient Internalization and  
997 Microtubule-Dependent Trafficking of a Ciliary Signaling Receptor from the Plasma  
998 Membrane to the Cilium." *Current Biology* 29 (17): 2942–2947.e2.  
999 <https://doi.org/10.1016/j.cub.2019.07.022>.
- 1000 Robinson, Robert C., Kirsi Turbedsky, Donald A. Kaiser, Jean-Baptiste Marchand, Henry N. Higgs,  
1001 Senyon Choe, and Thomas D. Pollard. 2001. "Crystal Structure of Arp2/3 Complex." *Science*  
1002 294 (5547): 1679. <https://doi.org/10.1126/science.1066333>.
- 1003 Rohatgi, Rajat, and William J Snell. 2010. "The Ciliary Membrane." *Current Opinion in Cell*  
1004 *Biology* 22 (4): 541–46. <https://doi.org/10.1016/j.ceb.2010.03.010>.
- 1005 Rosenbaum, J. L., J. E. Moulder, and D. L. Ringo. 1969. "Flagellar Elongation and Shortening in  
1006 *Chlamydomonas*. The Use of Cycloheximide and Colchicine to Study the Synthesis and  
1007 Assembly of Flagellar Proteins." *The Journal of Cell Biology* 41 (2): 600–619.  
1008 <https://doi.org/10.1083/jcb.41.2.600>.
- 1009 Saito, Masaki, Wataru Otsu, Kuo-Shun Hsu, Jen-Zen Chuang, Teruyuki Yanagisawa, Vincent  
1010 Shieh, Taku Kaitsuka, Fan-Yan Wei, Kazuhito Tomizawa, and Ching-Hwa Sung. 2017.  
1011 "Tctex-1 Controls Ciliary Resorption by Regulating Branched Actin Polymerization and  
1012 Endocytosis." *EMBO Reports* 18 (8): 1460–72.  
1013 <https://doi.org/10.15252/embr.201744204>.

- 1014 Sali, A., and T. L. Blundell. 1993. "Comparative Protein Modelling by Satisfaction of Spatial  
1015 Restraints." *Journal of Molecular Biology* 234 (3): 779–815.  
1016 <https://doi.org/10.1006/jmbi.1993.1626>.
- 1017 Spector, Ilan, Nava R. Shochet, Dina Blasberger, and Yoel Kashman. 1989. "Latrunculins—Novel  
1018 Marine Macrolides That Disrupt Microfilament Organization and Affect Cell Growth: I.  
1019 Comparison with Cytochalasin D." *Cell Motility* 13 (3): 127–44.  
1020 <https://doi.org/10.1002/cm.970130302>.
- 1021 Willox, Anna K., Yasmina M. E. Sahraoui, and Stephen J. Royle. 2014. "Non-Specificity of Pitstop  
1022 2 in Clathrin-Mediated Endocytosis." *Biology Open* 3 (5): 326–31.  
1023 <https://doi.org/10.1242/bio.20147955>.
- 1024 Wingfield, Jenna L, Ilaria Mengoni, Heather Bomberger, Yu-Yang Jiang, Jonathon D Walsh, Jason  
1025 M Brown, Tyler Picariello, et al. 2017. "IFT Trains in Different Stages of Assembly Queue  
1026 at the Ciliary Base for Consecutive Release into the Cilium." Edited by Erwin J G  
1027 Peterman. *ELife* 6 (May): e26609. <https://doi.org/10.7554/eLife.26609>.
- 1028 Winter, D. C., E. Y. Choe, and R. Li. 1999. "Genetic Dissection of the Budding Yeast Arp2/3  
1029 Complex: A Comparison of the in Vivo and Structural Roles of Individual Subunits."  
1030 *Proceedings of the National Academy of Sciences of the United States of America* 96  
1031 (13): 7288–93. <https://doi.org/10.1073/pnas.96.13.7288>.
- 1032 Wood, Christopher R., and Joel L. Rosenbaum. 2014. "Proteins of the Ciliary Axoneme Are  
1033 Found on Cytoplasmic Membrane Vesicles during Growth of Cilia." *Current Biology* 24  
1034 (10): 1114–20. <https://doi.org/10.1016/j.cub.2014.03.047>.
- 1035 Wu, Chien-Ting, Hsin-Yi Chen, and Tang K. Tang. 2018. "Myosin-Va Is Required for Preciliary  
1036 Vesicle Transportation to the Mother Centriole during Ciliogenesis." *Nature Cell Biology*  
1037 20 (2): 175–85. <https://doi.org/10.1038/s41556-017-0018-7>.
- 1038 Zuo, Xiaofeng, Wei Guo, and Joshua H. Lipschutz. 2009. "The Exocyst Protein Sec10 Is Necessary  
1039 for Primary Ciliogenesis and Cystogenesis In Vitro." *Molecular Biology of the Cell* 20 (10):  
1040 2522–29. <https://doi.org/10.1091/mbc.e08-07-0772>.
- 1041  
1042